Trajectory and Spacecraft Design for a Pole-Sitter Mission

Matteo Ceriotti,* Jeannette Heiligers,† and Colin R. McInnes‡
University of Strathclyde, Glasgow G1 1XJ, United Kingdom

This paper provides a detailed mission analysis and systems design of a pole-sitter mission. It considers a spacecraft that is continuously above either the North or South Pole and, as such, can provide real-time, continuous and hemispherical coverage of the polar regions. Two different propulsion strategies are proposed, which result in a near-term pole-sitter mission using solar electric propulsion and a far-term pole-sitter mission where the electric thruster is hybridized with a solar sail. For both propulsion strategies, minimum propellant pole-sitter orbits are designed. Optimal transfers from Earth to the pole-sitter are designed assuming Soyuz and Ariane 5 launch options, and a controller is shown to be able to maintain the trajectory under unexpected conditions such as injection errors. A detailed mass budget analysis allows for a trade-off between mission lifetime and payload mass capacity, and candidate payloads for a range of applications are investigated. It results that a payload of about 100 kg can operate for approximately 4 years with the solar-electric spacecraft, while the hybrid propulsion technology enables extending the missions up to 7 years. Transfers between north and south pole-sitter orbits are also considered to observe either pole when illuminated by the Sun.

Nomenclature

A	Area, m^2
$\mathbf{a}$	Acceleration vector, mm/s^2
AU	Astronomical Unit, $1.495978707 \cdot 10^8$ km
d	Earth to pole-sitter distance, km
$\mathbf{f}$	Dynamics function
J	Objective function
k	Specific performance of SEP, kg/kW
$\mathbf{K}$	Gain matrix
m	Mass
m_{dry}	Dry mass, kg

* Currently at University of Glasgow, Systems Power and Energy Division, School of Engineering, James Watt Building South, Glasgow G12 8QQ, United Kingdom. AIAA Member.
† Ph.D. Candidate, Advanced Space Concepts Laboratory, Department of Mechanical and Aerospace Engineering, 75 Montrose Street.
‡ Director, Advanced Space Concepts Laboratory, Department of Mechanical and Aerospace Engineering, 75 Montrose Street, AIAA Member.

m_{gimbal}	Gimbal mass, kg
m_{other}	Additional spacecraft subsystems mass, kg
m_{pl}	Payload mass, kg
m_{prop}	Propellant mass, kg
m_{rad}	Radiator mass, kg
m_{tank}	Propellant tank mass, kg
$m_{thruster}$	SEP thruster mass, kg
$n_{thrusters}$	Number of SEP thrusters
P	Power, W
P_d	Excess power, W
$\mathbf{Q}$	Weight matrix
$\mathbf{r}$	Position vector, km
$\mathbf{R}$	Weight matrix
t	Time, days or years
$\bar{t}$	Given instant of time
$t_{mission}$	Mission lifetime, days or years
$\mathbf{u}$	Control vector
$\mathbf{v}$	Velocity vector, m/s
w	Objective weight factor
W	Energy flux density of the Sun at 1 AU, 1367 W/m^2
$\mathbf{x}$	State vector
α	Cone angle, deg
β	Solar sail lightness number
δ_{eq}	Obliquity of the ecliptic, deg
δr_x	Error on position in x-direction, km
$\delta\mathbf{u}$	Feedback control
δv_z	Error on velocity in z-direction, m/s
$\delta\mathbf{x}$	State error
ε_{new}	Margin for new technologies
ε_{old}	Margin for well-proven technologies
η	Efficiency
ρ_{gimbal}	Proportionality constant for gimbal mass
σ	Areal density, g/m^2
σ^*	Critical sail loading, g/m^2
$\boldsymbol{\omega}$	Angular velocity vector, rad/year

Subscripts

0	At initial time, i.e. injection into pole-sitter orbit
f	At final time
max	Maximum value
r	Reference
s	Solar sail
SA	Solar array
SEP	Solar electric propulsion
TF	Thin film solar cells

Other notation

$\dot{\square}$	Differentiation with respect to time

I. Introduction

Spacecraft in geostationary orbit (GEO) have demonstrated the significant benefits offered by continuous coverage of a particular region. However, GEO platforms can only provide their services in the equatorial and temperate zones, where elevation angles are sufficiently high.

At higher latitudes, similar services are provided at present by mainly two types of conventional platforms: highly-eccentric, inclined orbits, or low or medium polar orbits.

The first class includes the well-known Molniya-type orbits: they exploit the oblateness of the Earth (effect of the J_2 term in the geopotential) to maintain the argument of the pericentre constant in time [1]. In order to achieve this condition, their inclination must be fixed at the critical value of 63.4°. This value is still relatively low to obtain a satisfactory coverage not only of the polar caps, but also of the high-latitude regions [2]. Due to their high eccentricity, the orbit apocentre is usually at a distance that is comparable to GEO, and therefore offers a hemispheric view of the Earth, albeit not centered in the pole. However, an intrinsic limitation is the impossibility of providing continuous coverage over time: despite that the spacecraft spends a significant fraction of its orbital period around the orbit apocentre, the viewing conditions of the poles change continuously, and there is an interval of time in which the spacecraft is at the pericentre and coverage is not available. With an orbital period of approximately 12 hours, it has been shown that from three to six Molniya spacecraft are necessary to provide satisfactory continuous coverage [3].

Recent research [4] has considered changing the critical inclination of the Molniya orbit to 90°, using a continuous solar electric propulsion (SEP) system for maintaining the orbit. However, continuous and so a constant polar view is still not available with a single spacecraft.

The second class of orbits largely consists of Sun-Synchronous orbits. Spacecraft in these orbits are used due to the high spatial resolution that they can provide. However, only a narrow swath is imaged at each polar passage, relying on multiple passages (and/or multiple spacecraft) for full coverage. For example, Landsat 7 (altitude of 705 km at 98.2°) completes just over 14 orbits per day, covering the entire Earth between 81 degrees north and south latitude every 16 days.[*] This results in a poor temporal resolution for the entire polar region, as different areas are imaged at different times, hence missing the opportunity to have a simultaneous and continuous real-time view of the pole. At present, these images are post-processed to make a composite image, which can be used, for example, for weather forecasting and wind vector prediction. However, the data that can be extracted is neither complete nor accurate [5].

[*] Landsat 7 Handbook, http://landsathandbook.gsfc.nasa.gov/ [Cited 12/09/2011]

To overcome these limitations, the ideal platform would be one with a continuous view of the poles for a long duration, or even better, one that is constantly above one of the poles, stationary with respect to the Earth, in the same way as a GEO spacecraft is stationary above one point on the equator. In this position, the footprint of the spacecraft will be constantly at the pole, in the same way as the footprint of a geostationary spacecraft is constantly at some longitude on the equator.

This spacecraft is known in literature as “pole-sitter”, which uses low-thrust propulsion to maintain a position along the polar axis (see Fig. 1). The pole-sitter is the only platform that can offer a truly continuous hemispheric view of one of the poles, enabling real-time imaging over the entire disc. The first study of this concept was apparently made by Driver [6] in 1980, although the author notes that the original idea belongs to the mathematician and writer Kurd Lasswitz from 1897.

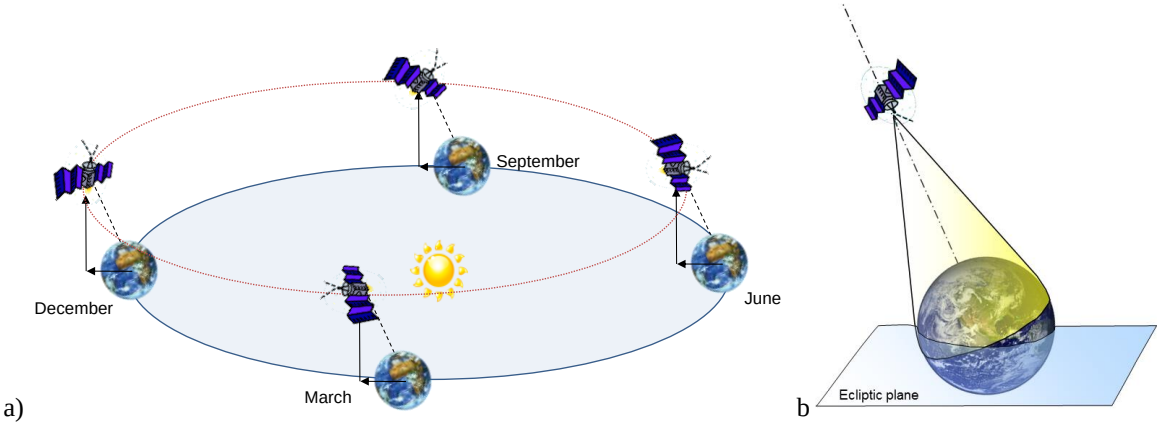

Fig. 1 Pole-sitter concept in (a) Sun-centered inertial frame and (b) Earth-centered frame.

In order to keep the pole-sitter spacecraft at a fixed position on the polar axis, a continuous acceleration has to be provided, to counterbalance mainly the gravitational attraction of the Earth and of the Sun. Driver proposed the use of solar electric propulsion (SEP). SEP is now a mature technology, but despite its high efficiency, the thrusting time and hence the mission duration is always limited by the mass of propellant on-board.

In order to avoid this drawback, some authors investigated the use of solar sailing [7] instead of SEP as a means to provide the continuous acceleration to continuously observe high-latitude regions. Novel families of non-Keplerian orbits (NKOs) [8] and artificial displaced equilibria were introduced, to provide similar services; the Statite [9] is a static solar sail spacecraft concept for polar communications, based on the surfaces of equilibrium for a solar sail in the circular restricted three-body problem [10]. However, due to the intrinsic limitation of the sail to provide an acceleration away from the Sun and limitations in realistic sail area-to-mass ratios, none of these concepts achieve satisfactory conditions for continuous coverage of high-latitude regions. This and other issues are discussed in detail in Ref. [2], together with a comparison of concepts for high-latitude observation.

In order to overcome the limitations of a platform based on a pure sail, hybrid propulsion has been proposed [11]. Hybridizing SEP and solar sailing is a comparatively recent idea [11], nevertheless research is flourishing in this field, investigating novel, interesting applications: artificial equilibria above L_1 in the Sun-Earth system for Earth observation [12], optimal interplanetary transfers to Venus and Mars [13, 14], displaced periodic orbits in the Earth-Moon system [15] and displaced NKOs for geostationary coverage [16].

In the hybrid system, at the cost of increased spacecraft and mission design complexity, the two propulsion systems complement each other, cancelling their reciprocal disadvantages and limitations. In principle, SEP can provide thrust in almost any direction (as long as the exhaust flow does not interfere with other spacecraft systems), and in particular towards the Sun, where the sail cannot. Similarly, the hybrid spacecraft can be seen as an SEP spacecraft, in which an auxiliary solar sail provides part of the acceleration, enabling a saving of propellant mass, and lowering the demand on the electric thruster, possibly with some intervals in which it could be turned off. In this sense, the hybrid spacecraft can be seen as a way to gradually introduce solar sails for space applications, and hence to reduce the advancement degree of difficulty [17] in the technology readiness level scale. Therefore, hybrid propulsion can in principle enable missions that are not feasible using only a solar sail and can extend the mission lifetime with respect to the pure SEP case.

Regardless the type of propulsion, the acceleration required by a pole-sitter spacecraft increases dramatically as the spacecraft is stationed closer to the Earth, and reasonable values of acceleration are obtained only if the Earth-spacecraft distance is of the order of millions of kilometers [6, 18]. Nevertheless, the advantage of having a static or quasi-static platform is such that these concepts are worth considering and investigating [19]. Although high-bandwidth telecommunications and high-resolution imagery are difficult due to the large Earth-spacecraft distance, a number of novel potential applications are enabled, both in the fields of observation and telecommunications, which will be described later in the paper.

Due to these potential benefits, and with the aim of increasing mission lifetime, the authors have undertaken an extensive investigation focused on the concept of a hybrid-propulsion pole-sitter. Recent publications detailed different parts of the mission: the generation of optimal hybrid pole-sitter orbits [18], the hybrid system mass budget [20], the design of optimal transfers to the pole-sitter orbit from LEO [21], and the design of optimal north-to-south transfers [22]. These papers presented in detail the trajectory optimization process for each one of the mission phases. However, a complete end-to-end mission design, including the trajectory integration, the payload selection and consequently the spacecraft sizing, has not been presented.

The intent of this paper is to build upon the methodologies used in the previous works, and by using the trajectory optimization tools developed previously, to design a complete mission for a realistic pole-sitter spacecraft, covering one

pole continuously or either pole seasonally. We will consider two launcher options (Ariane and Soyuz) and for each one, compare two spacecraft propulsion options (SEP or hybrid sail-SEP), thus creating four different mission scenarios. In addition, suitable payloads will be identified for the mission, and through a detailed and conservative systems design and mass budget, the mass and the lifetime of the spacecraft, for the different scenarios, will be determined. Finally, a controller is designed and simulated to quantify the effects of the orbital perturbations and possible launcher injection errors.

II. Mission Description

A. Mission Phases

The complete pole-sitter mission is split into different phases, which will be described in detail and designed in the following sections. The phases are schematically represented in Fig. 2.

The mission starts with a launch and transfer phase. This phase begins with the spacecraft injected into a low Earth orbit (LEO) by the launcher; the type and size of the LEO depends on the launcher used. The launcher upper stage provides number of impulsive maneuvers, before jettisoned; the spacecraft continues the transfer using its own low-thrust propulsion system, up to the injection point into the pole-sitter orbit.

At this point, the operational phase begins. The operational phase is the one in which the spacecraft is stationed along the polar axis of the Earth, maintaining its nominal pole-sitter orbit. This is obviously the most important phase of the mission, and its duration shall be maximized.

Since each pole is lit only 6 months per year, it is an option, especially for observations in the visible part of the spectrum, to transfer the spacecraft from a North Pole operational orbit to a symmetric orbit below the South Pole, and vice-versa, according to their lighting conditions. Therefore, an additional north-to-south transfer phase is designed. This phase can be inserted at appropriate points along the nominal orbit to enable the transfer to the other pole, where a symmetric operational orbit can be followed.

These three phases will be described and designed sequentially, starting from the operational phase, which defines the optimal nominal orbit. Then, the transfer from Earth to this orbit will be designed. The optimization of the transfer allows the determination of the maximum mass at the pole-sitter orbit injection, and therefore the spacecraft can be sized and the lifetime assessed. Finally, the north-to-south transfers will be designed, between optimal pole-sitter orbits.

The design of the three phases requires the solution of optimal control problems, which are solved numerically using a direct method based on pseudospectral transcription, implemented in the tool PSOPT [23], and the non-linear programming problem is solved through IPOPT (interior point optimizer, [24]).

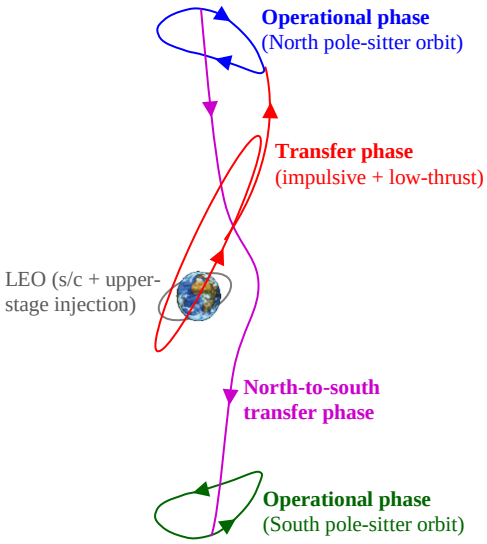

Fig. 2. Representation of the mission phases.

1. Trajectory models

For the transfer and operational phases we consider a three-body problem in which the spacecraft is subject to the gravitational attraction of both the Earth and the Sun. This choice is made since the gravity of the Earth and the Sun are both important for a practical pole-sitter. In particular, we use the well-known circular restricted three-body problem (CR3BP), which describes the motion of the spacecraft, of negligible mass, under the influence of the Sun and Earth (the *primaries*) that rotate in circular motion around each other (at a constant distance of 1 Astronomical Unit, AU). The reference frame is synodic, with its origin at the center-of-mass of the system, the x-axis passing through the Sun and the Earth, and oriented towards the latter, and the z-axis perpendicular to the ecliptic plane, see Fig. 3. The equations of motion for the spacecraft can be found in Ref. [18].

Note that the launch phase, which occurs close to the Earth, will be modeled using a two-body approach. Details of this model will be given in Section III.B.

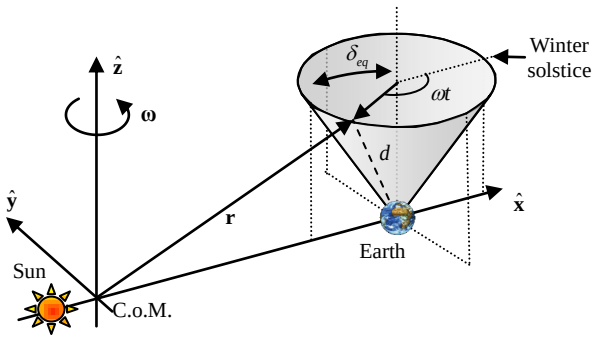

Fig. 3 Synodic reference frame of the restricted three-body problem and pole-sitter reference.

B. Spacecraft Propulsion Options

We consider two different spacecraft architectures. The first is a pure SEP spacecraft, in which solar electric propulsion is used to provide the acceleration required throughout the mission. The spacecraft complexity is relatively low in this case, due to the high TRL of this type of propulsion system. The second is a more advanced, long-term spacecraft that exploits both solar sail and solar electric propulsion on the same bus.

1. Pure SEP

The pure SEP spacecraft can be considered as a conventional spacecraft with deployable solar arrays to power the propulsion system. Usually, the solar panels can be rotated along their longitudinal axis, so as to modulate the power delivered according to the instantaneous need of the spacecraft. The thruster is assumed to be rigidly connected to the spacecraft bus, and the thrust vector is steered by changing the attitude of the spacecraft (the instruments can be mounted on a gimbal).

The key technology parameters of an SEP thruster are the maximum thrust that it can provide, usually in the order of a fraction of a Newton, and its specific impulse. In this paper, we assume that the maximum thrust is used to size the SEP system, as will be explained later, and a fixed specific impulse of 3200 s is conservatively assumed, based on current ion engine technology (existing NSTAR/DS1 [25] or EADS/Astrium RIT-XT [26]). It is foreseen that this specific impulse allows levels of thrust suitable for the spacecraft and mission under consideration.

Since the fuel mass consumption is directly related to the magnitude of the thrust, in general we will try to find trajectories that minimize propellant consumption, in order to maximize the mission lifetime, or alternatively, to maximize the payload mass for a given lifetime.

2. Hybrid Sail and SEP

In this scenario, we envisage the use of a spacecraft that combines solar sailing and SEP. As noted earlier, this adds system complexity, but it can be advantageous in terms of mission lifetime, as it will be shown in this paper.

The hybrid spacecraft has a bus from which the sail is deployed, and thus the sail is rigidly connected to it (see Fig. 4). We assume that the sail can be steered, with relatively modest angular acceleration, by using the attitude control system of the spacecraft. The SEP thruster is mounted on a gimbal system, because it is required that the SEP thrust vector can steer independently of the sail orientation, for control purposes. Furthermore, the SEP system requires electrical power in order to operate. In conventional spacecraft, this is collected through solar arrays that are hinged on the spacecraft bus and can be

oriented towards the Sun when power is needed. This type of architecture would be difficult to implement due to the presence of the sail. We instead envisage a layer of thin film solar cells (TFSC) which partly occupy the sail surface, similarly to the IKAROS spacecraft [27].

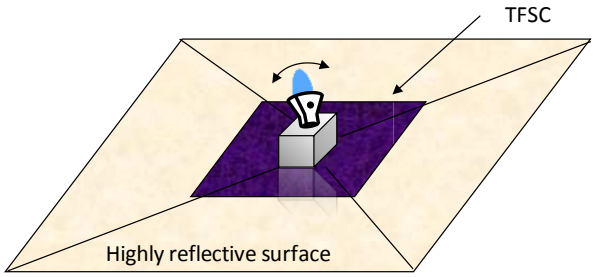

Fig. 4 Hybrid spacecraft with sail, thin film solar cells and steerable thruster.

We assume a partially reflective, partially absorbing solar sail (optical sail model) of total area A_s, such that the solar radiation pressure generates an acceleration with a component perpendicular to the sail and one parallel to it [11, 12]. The sail acceleration is proportional to the parameter β, the *system lightness number*, which is a function of the sail loading $\sigma = m/A$ of the spacecraft (spacecraft mass over total sail area):

$$\beta = \sigma^* / \sigma \tag{1}$$

with $\sigma^* \cong 1.53 \cdot 10^{-3}$ kg/m^2 the critical sail loading. However, β can also be defined as the ratio of the maximum solar radiation pressure acceleration at 1 A.U. (*sail characteristic acceleration*) to the gravitational acceleration. Note that β varies during the mission, because of the decrease in spacecraft mass *m* due to SEP propellant consumption. We therefore introduce the value $\beta_0 = \beta \frac{m}{m_0}$, constant, in which the subscript "0" refers to the parameters at the injection into the pole-sitter operational orbit, when the time is t_0. Note that the pure SEP spacecraft can be considered as a particular hybrid system with $\beta = \beta_0 = 0$. Values of β up to 0.05 can be assumed for a near-term hybrid system [28]. Recent solar sail demonstrators, however, had considerably lower lightness numbers: JAXA's IKAROS [29] has a 20-m-diagonal square sail and weighs 350 kg (β = 0.001), while NASA's NanoSail-D2 [30] is 4 kg for 10 m^2 (β = 0.003).

In the hybrid spacecraft, the TFSCs are assumed to cover an area $A_{TF} = 0.05A$ on the sail. This area ratio is a conservative estimation based on previous studies [12] and the IKAROS mission [29], and it is used to compute the optimal orbits. The actual value of this area depends on the spacecraft technology parameters, as well as the selected orbit, and will be computed in Section V.A.

Another important technological parameter of a sailcraft is the areal density of the sail assembly, σ_s. It measures the mass of the sail per unit surface area, and it is expected that technological developments [28] should enable sails of 10 g/m^2 in the near future. Ultra-thin (around 2 μm of thickness) sails are expected in the mid- to far-term timeframe [31] and can lead, for large sails, to sail loadings of the order of 5 g/m^2.

Given these considerations, the value of β_0 for the hybrid scenario can be decided following the study in Ref. [20]. That work showed that, if a sail assembly areal density of 10 g/m^2 is considered, then the hybrid spacecraft is beneficial only if very long missions are considered (i.e. lifetime > 7 years). Instead, considerable mass saving (or extended lifetime) is expected considering a hybrid system with $\sigma_s = 5 \text{ g/m}^2$ (or below). Furthermore, for this value, it is found that that $\beta_0 = 0.035$ represents the lightness number in which the spacecraft initial mass, for a given payload, is lowest over a range of mission lifetimes. For these reasons, we select for this scenario: $\beta_0 = 0.035$, $\sigma_s = 5 \text{ g/m}^2$.

III. Trajectory Design

A. Pole-Sitter Operational Orbits

In this section, we design an optimal pole-sitter orbit for each of the two types of spacecraft under consideration.

A pole-sitter spacecraft is stationed along the polar axis of the Earth. We can consider that the direction of the polar axis of the Earth is inertially fixed while the Earth is orbiting the Sun (neglecting the nutation of the polar axis and the precession of the equinoxes). In the synodic ecliptic reference frame, the same axis rotates with a motion of apparent precession, due to the obliquity of the ecliptic: its angular velocity is $-\omega = -2\pi/\text{year}$ (see Fig. 3). Therefore, the polar axis spans a full conical surface every year, in a clockwise direction (refer again to Fig. 3). The cone half angle is the tilt of the axis relative to the ecliptic, i.e. $\delta_{eq} = 23.5 \text{ deg}$. The position of the spacecraft is to be constrained to follow the clockwise apparent precession of the polar axis, and hence maintain the pole-sitter condition. Without loss of generality, we consider the time $t_0 = 0$ as the winter solstice, and therefore the spacecraft's position is function of the only free variable $d(t)$, a function of time which represents the distance of the spacecraft from the Earth. Fig. 3 represents a particular pole-sitter orbit in which $d(t)$ is constant.

An optimal pole-sitter orbit is defined as the one that minimizes the propellant consumption of the spacecraft, while maintaining the pole-sitter condition at any time, and being one-year periodic. The implicit approximation that is made here is that the optimal control problem is solved only for the first year (or period) of the mission, and the same trajectory is then used for following years. In reality, a fully optimized trajectory would change year by year, due to the change in mass of the

spacecraft. In other words, the optimal control problem should be solved not only for one year, but for the entire mission lifetime at once. However, the lifetime cannot be determined at this stage, and the full optimization would result in only minor differences and therefore it is not used in this paper.

Details of the optimization process are presented in Ref. [18]. As noted, the optimal control problem is solved with PSOPT, and the first guess is found through an inverse approach, in which a trajectory satisfying the constraints is assumed (although non-optimal) and the controls for this trajectory are derived through a semi-analytical procedure.

The mass of the spacecraft appears in the equations of motion. In Ref. [18] the initial mass was set arbitrarily to 1000 kg, but in this work the initial mass is not known: it depends on the launcher capability and the transfer phase, which in turn depend on the operational orbit. However, it can be shown that if the SEP system can provide the acceleration required by the optimal trajectory at any time (i.e. the constraint on the maximum thrust is not active), then the problem is fully scalable on the initial mass, and it can be solved in terms of mass fraction of an arbitrary initial mass. This consideration allows to find optimal pole-sitter orbits (with no thrust limit) independently of the initial spacecraft mass.

In the optimization process, the maximum distance from the Earth is limited to $d_{max} = 0.01831\,\mathrm{AU}$, i.e. 2.74 million km, in order to prevent the trajectory from going too far away from the Earth, thereby excessively decreasing the spatial resolution for instruments or the data bandwidth of the platform. In fact, it was found (see Ref. [18]) that optimal, unconstrained trajectories move further away from the Earth in summer, which is the period in which observations in optical wavelength can be better performed due to the North Pole being lit.

The result of the optimization, for the two scenarios, is presented in Fig. 5. Note that all the figures showing the orbits (or later on in the paper, the transfers) employ a Sun-Earth synodic reference frame centered at the Earth rather than at the Sun-Earth barycenter for interpretation purposes. As Fig. 5 (a) and (b) show, the optimal SEP-only path is essentially symmetric around spring and autumn, and the spacecraft is closest to the Earth at the summer and winter solstices. Instead, in the hybrid case, the spacecraft is closest to the Earth in winter and farthest in summer: the constraint on the maximum distance is active across the summer solstice for approximately 150 days. Fig. 5 (b) also highlights that the SEP spacecraft distance to Earth varies between 2.3457 and 2.7391 million km, while for the hybrid case it varies between 2.0480 and 2.7391 million km. Fig. 5 (c) instead plots the modulus of the SEP acceleration as function of time in the two scenarios, which shows that the hybrid case needs less acceleration due to the contribution of the sail.

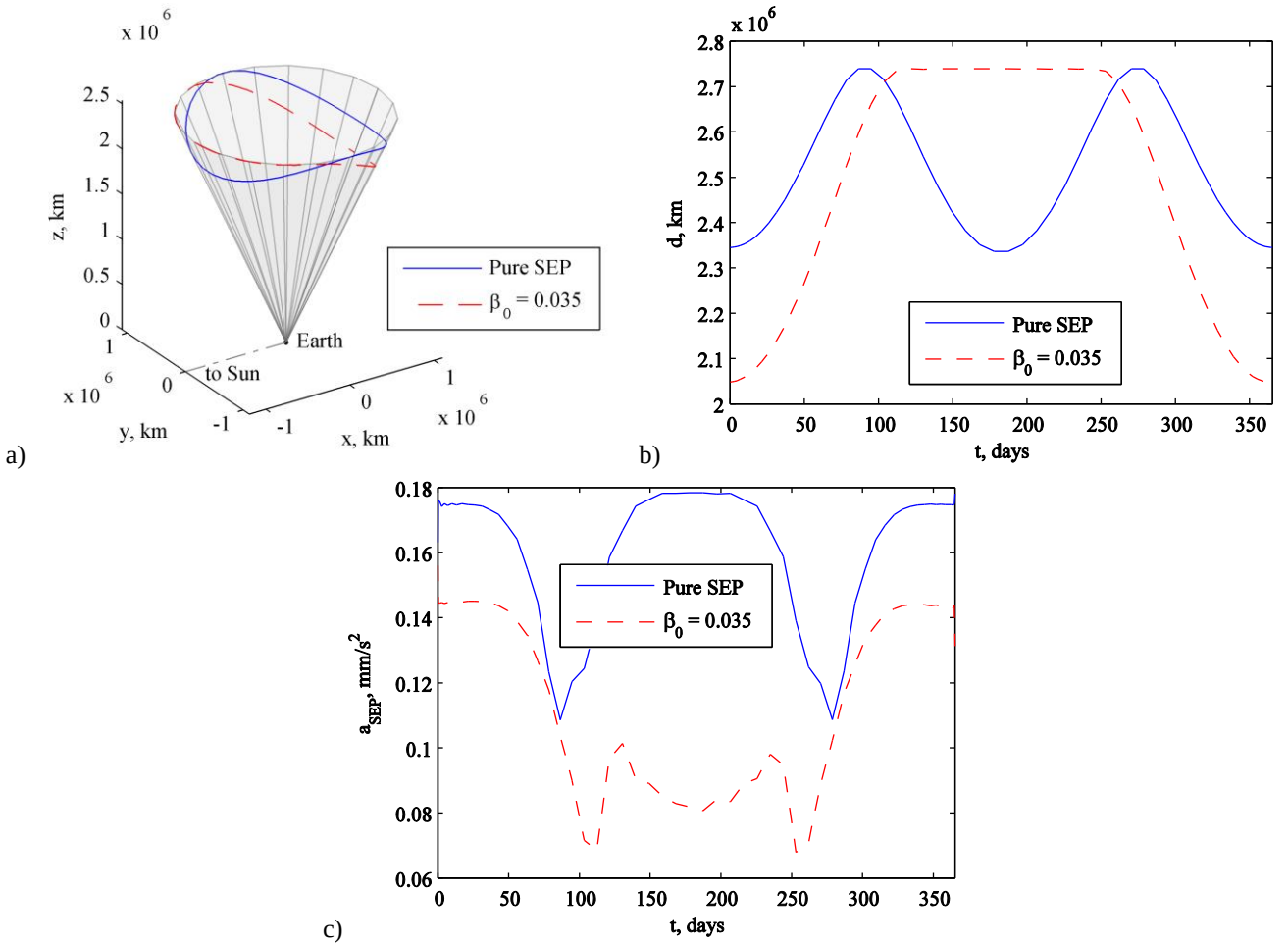

Fig. 5 Fuel-optimal pole-sitter orbits for the pure SEP case and the hybrid case. (a) Optimal trajectories in the synodic reference frame. (b) Distance from the Earth. (c) SEP acceleration (magnitude) required.

Since we stated that the problem is scalable with initial mass, we can then say that the thrust needed can be found multiplying the SEP acceleration in Fig. 5 (c) with the mass, once the mass at injection is known. Due to the periodicity of the orbit, the maximum thrust is achieved in the first period, when the spacecraft mass is highest; observing the acceleration over one period in Fig. 5 (c), we can also infer that the maximum thrust is required at the winter solstice, which coincides with pole-sitter injection, as will be shown in the next section.

This value of the maximum thrust is the one that the SEP system shall provide for maintaining the orbit, and is also used to size the propulsion subsystem itself. For example, for a spacecraft of mass 1000 kg at injection, the maximum SEP thrust would be 170 mN for the pure SEP system, and 144 mN for the hybrid system.

B. Launch and Transfer Phase

In order to find the maximum mass that can be inserted into the operational orbit, this section investigates optimum transfers from LEO up to insertion into the pole-sitter orbit. The transfer is modeled by distinguishing between a launch

phase and a transfer phase, as shown in Fig. 2. The launch phase is designed as an impulsive, two-body Soyuz or Ariane 5 upper-stage transfer from a fixed inclination low-Earth parking orbit up to insertion into the transfer phase. This transfer phase is modeled in the Earth-Sun three-body problem and either pure SEP or hybrid propulsion is used in the transfer, depending on the system architecture. The overall objective is to maximize the mass upon insertion into the pole-sitter orbit, assuming the full launch vehicle capacity to LEO is used. To this end, PSOPT solves the optimal control problem in the transfer phase and patches the launch phase to the transfer phase in an end-point constraint. More details on this approach as well as the generation of suitable initial guesses can be found in Ref. [21]. However, note that in that work the optimization considers a fixed mass upon injection into the pole-sitter orbit (1000 kg) and minimizes the mass required in LEO, while the approach considered in this paper fixes the mass in LEO, while maximizing the mass upon insertion.

Hereafter some details of the Soyuz and Ariane 5 launch phases will be given, followed by a short description of the optimal control problem to be solved and the results obtained.

1. Soyuz Launch Vehicle

In previous work [21], a launch vehicle model was developed that was shown to accurately match the Soyuz launch vehicle performance provided by the Soyuz manual in Ref. [32]. The model assumes that the first three stages of the Soyuz are launched from Baikonur and are used to reach a LEO with an altitude of 200 km and with one of four reference inclinations: 95.4, 70.4, 64.9 and 51.8 deg. Depending on the inclination, the Soyuz launch vehicle can provide payload masses of 6275 to 7185 kg respectively. From the parking orbit, any remaining inclination and altitude changes can be provided by the Fregat upper-stage through a two-body Hohmann transfer to the final target orbit, where any inclination change is distributed over the first (apogee raise) and second (perigee raise) Fregat burns. Hohmann transfer formulas [33] and the rocket equation are subsequently used to provide the mass that can be delivered to this final target orbit (or equivalently to the start of the transfer phase). A validation of this launch model is given in Ref. [21].

In principle, any of the four parking orbit inclinations could be used for the pole-sitter transfer. Because the pole-sitter can be viewed as having an inclination of 90 degrees, one could expect that, the closer the inclination of the parking orbit is to the inclination of the pole-sitter, the better the performance in terms of mass at pole-sitter injection. However, the smaller the parking orbit inclination, the better the Soyuz performance in the parking orbit. Initial results have indeed shown that this higher mass in the parking orbit eventually translates into a larger mass at injection than when considering a parking orbit with an inclination closer to the inclination of the pole-sitter orbit. Therefore, the remaining analyses in this section will assume a parking orbit inclination of 51.8 degrees.

An overview of the final parking orbit parameters and details of the Soyuz Fregat upper-stage are given in Table 1.

2. Ariane 5 Launch Vehicle

For comparison purposes, and also because less detailed information is available in the literature for the performance of the Ariane 5 launch vehicle than for the Soyuz launch vehicle, it is assumed that a similar launch strategy can be adopted for the cryogenic upper-stage (ESC-A) of the Ariane 5. However, the parking orbit is assumed to have an altitude of 400 km and an inclination of 51.6 deg inclination, for which it is known that Ariane 5 can deliver 19 t [34]. Other details of the Ariane 5 upper-stage are provided in Table 1.

Table 1 Soyuz and Ariane 5 parking orbit and launch vehicle specifications

Launcher	Parking orbit			Upper stage		Adapter
	Altitude, km	Inclination, deg	Performance, kg	Mass, kg	Specific impulse, s	Mass, kg
Soyuz	200	51.8	7185	1000	330	100
Ariane 5	400	51.6	19000	4540	446	160

3. Results

Fig. 6 shows the transfers for both SEP and hybrid cases. The figure shows that the optimal transfers inject the spacecraft at winter solstice, i.e. at the point closest to the Earth along the pole-sitter orbit. Note that, due to the symmetry of the SEP pole-sitter orbit with respect to an imaginary *y*-*z* plane, a similar, equally optimal transfer that injects at summer solstice can be found. More details on the optimal transfers, including the maximum thrust magnitude and mass injected into the pole-sitter orbit can be found in Table 2.

Comparing the performances of the SEP case using the Soyuz and Ariane 5 launch vehicles shows an increase in the mass injected into the pole-sitter orbit by a factor 2.9 for an Ariane 5 launch: 1535 kg versus 4432 kg. A similar increase can be observed for the maximum thrust magnitude. Because the maximum thrust magnitude is allowed to scale with the increase in the injected mass that the Ariane 5 launch can establish, the results in Fig. 6 show a very clear scalability of the transfer. Any differences between the two transfers can be attributed to the slightly different parking orbits from which the transfer is initiated.

The results for the SEP case are used as initial guess for the hybrid transfer. Since the SEP and hybrid pole-sitter orbits are not the same, a direct comparison of the performances of the transfers using the two propulsion techniques cannot be made. However, the mass injected into the hybrid pole-sitter orbit is larger than for the SEP case: an increase of 58 kg for a Soyuz launch and an additional 160 kg for an Ariane 5 launch. Part of this better performance is due to the smaller Earth to pole-sitter distance at winter solstice (i.e. upon injection) for the hybrid pole-sitter orbit. However, part is also due to the smaller propellant consumption in the transfer. This becomes clear from comparing the thrust profiles in Fig. 6 (b). Due to

the contribution of the sail, the hybrid case allows for a significantly shorter thrust arc. This comes however at the cost of a much longer time of flight than the optimal SEP transfer, see also Table 2. The reason for this is the fact that, during the optimal SEP transfer, the SEP thruster mainly provides a thrust in the direction of the Sun, which the sail is unable to generate. The result for the hybrid case is therefore the alternative, longer path. Note that during this longer path, the sail is optimally used by mainly providing a force directed radially away from the Sun. The same trajectory performed with only an SEP thruster would therefore require a much longer thrust arc than the optimal short SEP transfer presented in Fig. 6 (b) and would be suboptimal.

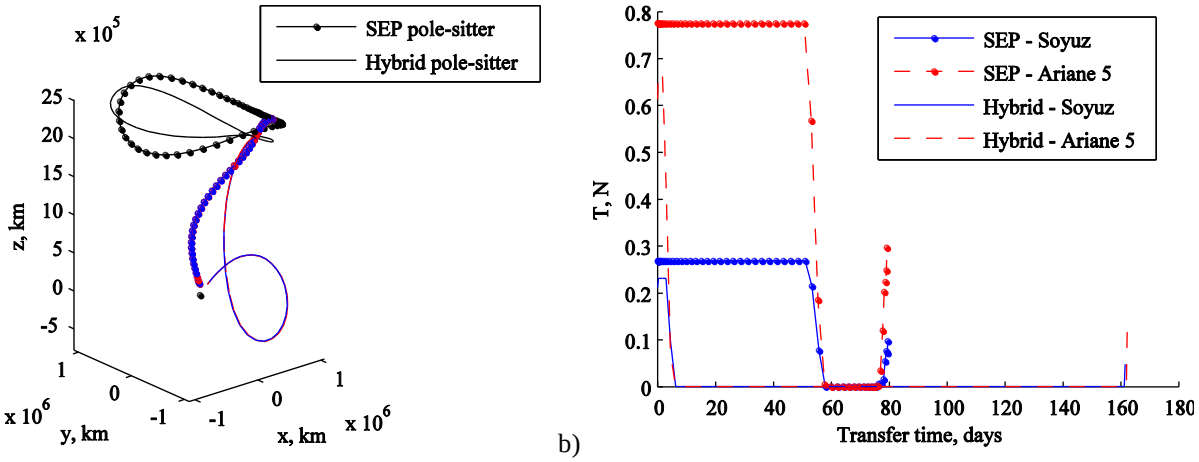

Fig. 6 Optimal transfers for SEP and hybrid propulsion with Soyuz and Ariane 5 launches. (a) Transfer in synodic reference frame. (b) Thrust profile.

Table 2 Results for the optimization of transfer to SEP and hybrid low-thrust pole-sitter orbits including the maximum SEP thrust magnitude and the mass injected into the pole-sitter orbits.

Architecture	Launcher	T_{max} , N	m_0 , kg	Time in transfer phase, days
SEP	Soyuz	0.269	1537	79.5
SEP	Ariane 5	0.775	4439	79.1
Hybrid	Soyuz	0.231	1595	161.4
Hybrid	Ariane 5	0.667	4599	162.2

C. Transfers between North and South Poles

Due to the tilt of the Earth's polar axis with respect to the ecliptic plane, the North and South Poles are alternately situated in darkness for 6 months per year. For observations performed in the visible part of the spectrum (e.g. using the SSI, HRI or EPIC instruments of Table 5), this significantly constrains the mission scientific return. Therefore, an additional transfer phase is introduced that allows the pole-sitter spacecraft to change between pole-sitter orbits above the North and South Poles before the start of the Arctic and Antarctic winters, see Fig. 2. For that, the SEP and hybrid pole-sitter orbits

shown in Fig. 5 are mirrored in the ecliptic plane. Viewed in the synodic frame, the Poles are illuminated when the spacecraft is in the Sun-ward part of the pole-sitter orbit, see Fig. 7. Ideally, this means that the pole-sitter spacecraft would follow the north pole-sitter orbit from March to September and the south pole-sitter orbit from September to March. Clearly in reality this is not feasible since some time needs to be allowed for the spacecraft to transfer from north to south and vice-versa.

Transfers between north and south pole-sitter orbits are applied in this section to the optimal SEP and hybrid pole-sitter orbits of Fig. 5. Also, for both propulsion strategies, both the Soyuz and Ariane 5 launch cases will be considered together with the corresponding values for the maximum thrust magnitude as provided in Table 2.

The work in Ref. [22], in which more details can be found, showed that two types of transfers can be considered: a short transfer that takes less than half a year and a long transfer that takes between half a year and one year. In order to maximize the observation time during the mission, this work will only consider the short transfer, which means that the departure and arrival windows for a north-to-south transfer are as indicated in Fig. 7. Departure thus takes place between summer and autumn (June – September), while arrival takes place between autumn and winter (September – December), where this paper conventionally refers to the seasons in the northern hemisphere.

Note that due to the symmetry of the problem, the optimal transfers from north to south can also be used to transfer from south to north. For that, it is assumed that the lower mass at the start of the south-to-north transfer (or any subsequent transfer) does not influence the trajectory to great extent.

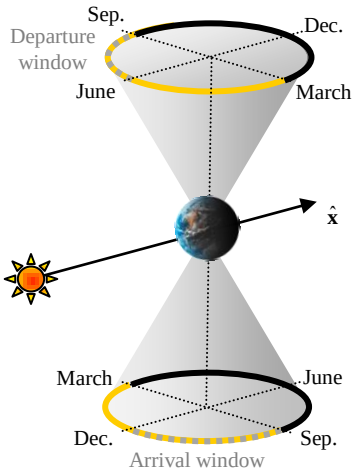

Fig. 7 Schematic of dark (black line) and light (yellow line) conditions on the North and South Poles during the year and departure and arrival window (dotted) for a north-to-south transfer.

The transfers are optimized to minimize a weighed sum of the propellant consumption and the time of flight through the objective function:

$$J = \frac{m_{t,0} - m_{t,f}}{m_{t,0}} + w \frac{t_{t,f} - t_{t,0}}{365.25 \text{ days}} \tag{2}$$

with the subscripts '$t,0$' and 't,f' indicating the start and end of the transfer. Clearly, for $w = 0$ the minimum propellant case is considered.

The optimal control problem is once again solved with PSOPT, with initial guesses provided by a shape-based approach. End-point constraints are included to ensure that the initial and final conditions coincide with the north and south pole-sitter orbits in the departure and arrival windows indicated in Fig. 7, including the mass at the start of the transfer. This mass is computed by considering that the north-to-south transfer takes place in the first year of the mission and after injection of the masses provided in Table 2 at winter solstice.

1. Results

The results for the pure SEP case are shown in Fig. 8, where the following values for the weight factor are used: $w = [0 \quad 0.25 \quad 0.5 \quad 1.0 \quad 1.5]$. The figure clearly shows a resemblance between the Soyuz and Ariane 5 cases, once again indicating the scalability of the transfer with the mass. As indicated before, this is a result of the fact that the maximum SEP thrust magnitude scales proportionally with the increase in the injected mass that the Ariane 5 launch can establish, see Table 2.

Fig. 8b furthermore shows the gain in observation time per pole that can be achieved by increasing the weight factor. For the values considered here, observation times of up to 94 days per Pole can be achieved. This comes, however, at the cost of an increase in the propellant consumption as shown in Fig. 8c. This figure also includes the propellant consumption in the pole-sitter orbit itself and can therefore provide insights into how demanding the north-to-south pole-sitter transfers are. It becomes clear that, depending on the value for the weight, the transfer can provide a saving in propellant consumption, which can be used to significantly extend the mission lifetime of the pure SEP mission. Analogous results as those in Fig. 8 can be obtained for the hybrid case, see Fig. 9. The only clear difference is the better performance of the minimum propellant case (i.e. $w = 0$) in terms of propellant consumption. However, as a consequence, the observation time per pole is poor.

This is shown in Fig. 10, which provides the mass profile throughout the pole-sitter mission (SEP and hybrid, Soyuz launch) when the north-to-south transfers are taken into account seasonally and when they are not. The figure clearly shows the gain in propellant consumption that the transfers can establish. For example, for the SEP case and $w = 0$ the gain is 279.6 kg after 5 years. Increasing the weight factor leads to smaller gains and for $w = 1.5$ even a small loss of 45.3 kg can be observed after 5 years.

Finally, note that the transfers pass in front of the Sun-lit side of the Earth (close to the Lagrange point L_1). Potentially, this enables the payload on the spacecraft to perform some additional science, even during the transfers, in a similar way as the NASA DSCOVR mission, a stationary Earth observer designed to be located at L_1.

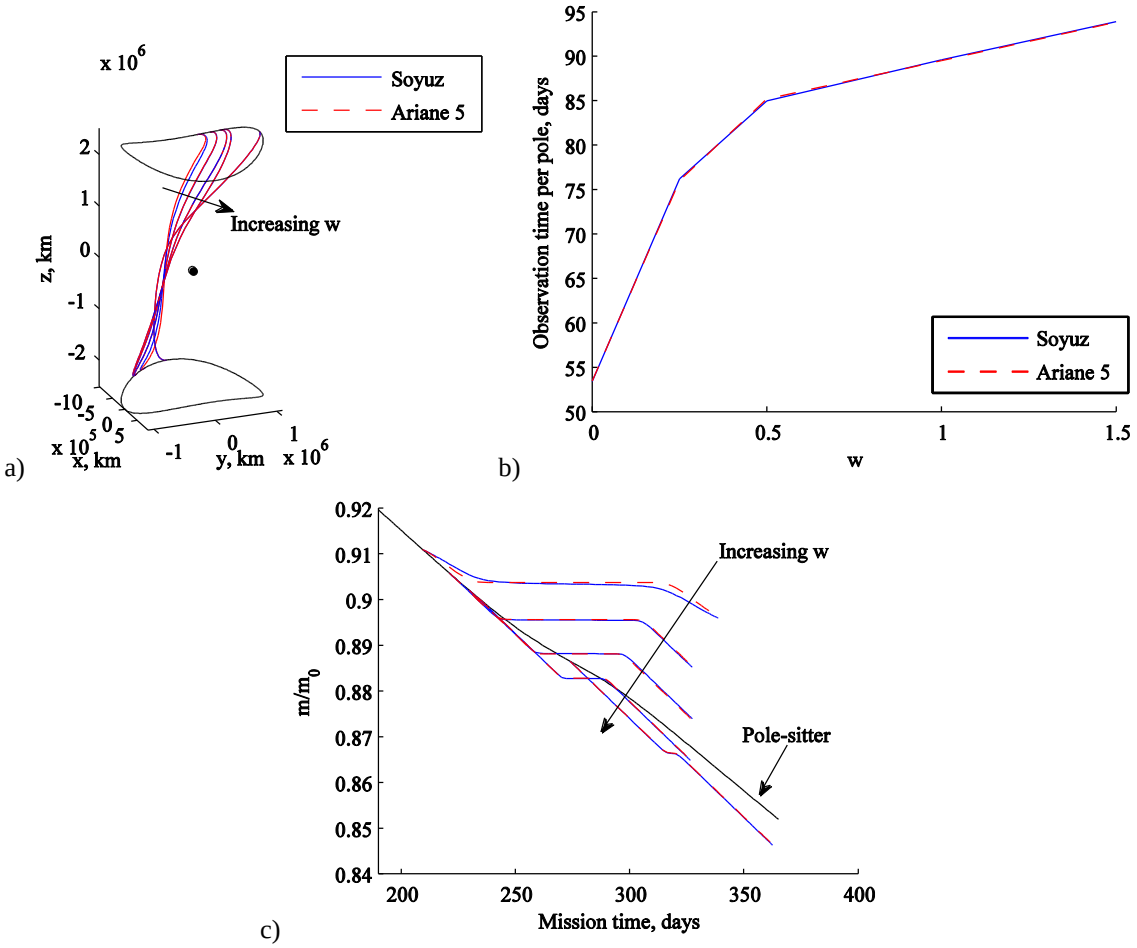

Fig. 8 Optimized, pure SEP north-to-south pole-sitter transfers for different values of the objective weight. (a) Transfers in the synodic reference frame. (b) Observation time per Pole as a function of the weight factor. (c) Ratio of current mass and mass at start of mission as a function of the mission time.

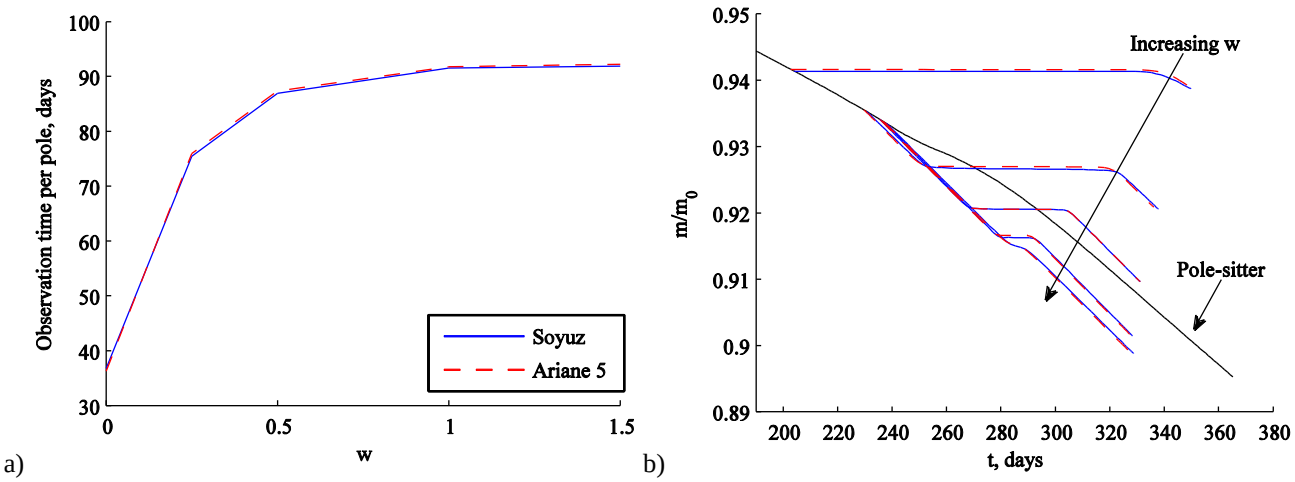

a) b)

Fig. 9 Optimized, hybrid north-to-south pole-sitter transfers for different values of the objective weight. (a) Observation time per Pole as a function of the weight. (b) Ratio of current mass and mass at start of mission as a function of the mission time.

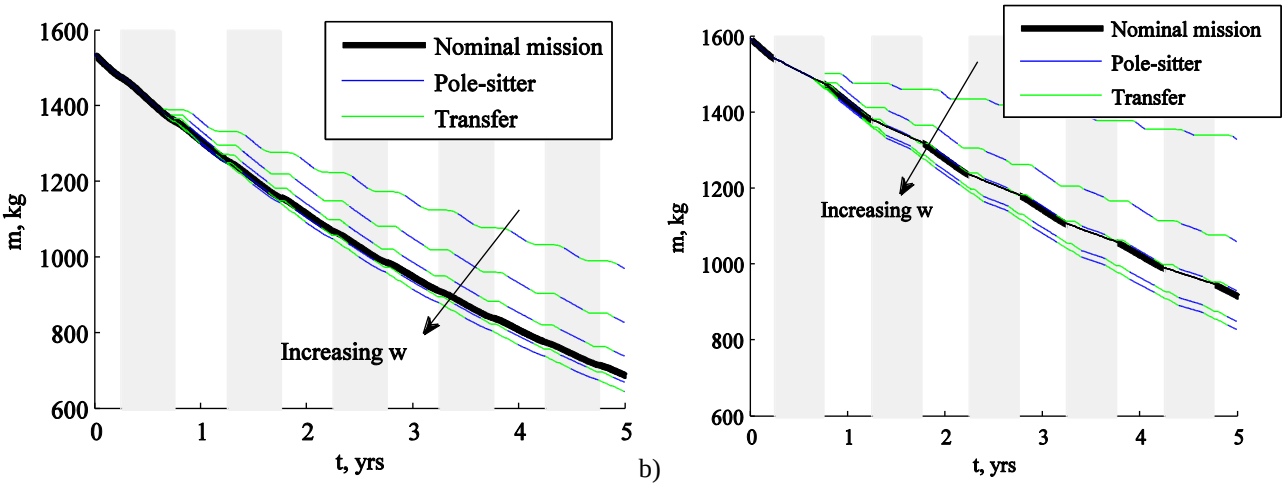

a) b)

Fig. 10 Mass profile throughout the pole-sitter mission (Soyuz launch) for SEP (a) and hybrid propulsion (b), including the north-to-south pole-sitter transfer for different values of the objective weight. Shaded areas highlight the half of the year when the North Pole is lit.

D. Overall Trajectory

Finally, to illustrate the full mission profile, Fig. 11 and Fig. 12 represent the trajectory of the pole-sitter spacecraft, including the launch phase, operational phases and north-to-south transfers. Fig. 11 refers to the pure SEP mission, Fig. 12 to the hybrid propulsion one. Both figures represent the Ariane 5 option; the trajectory followed by the Soyuz option is very similar. In each figure, the plot (a) is in an Earth-centered synodic reference frame (Earth and Lagrange points L_1 and L_2 are represented with dots), while the plot (b) is in an inertial, Sun-centered reference frame (the Sun represented with a dot, and the orbit of the Earth with a solid black line). Note that in plots (b) the z-direction is not to scale with x and y, in order to

appreciate the out-of-plane displacement of the pole-sitter, which would otherwise be too small with respect to the orbit of the Earth.

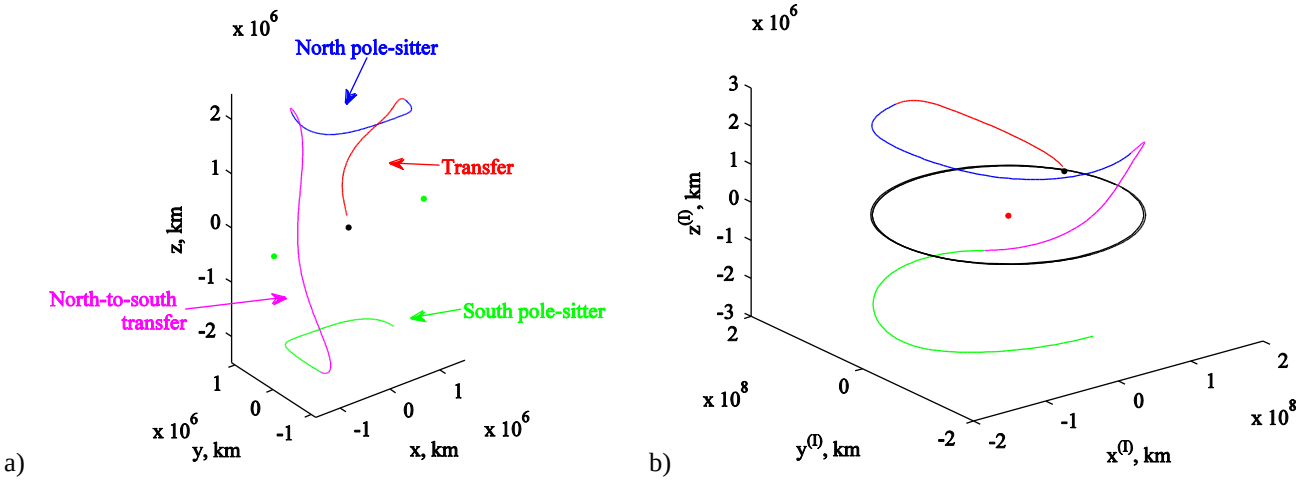

Fig. 11 Pure SEP mission trajectory (Ariane 5 launch) in synodic reference frame (a) and inertial Sun-centered reference frame (b).

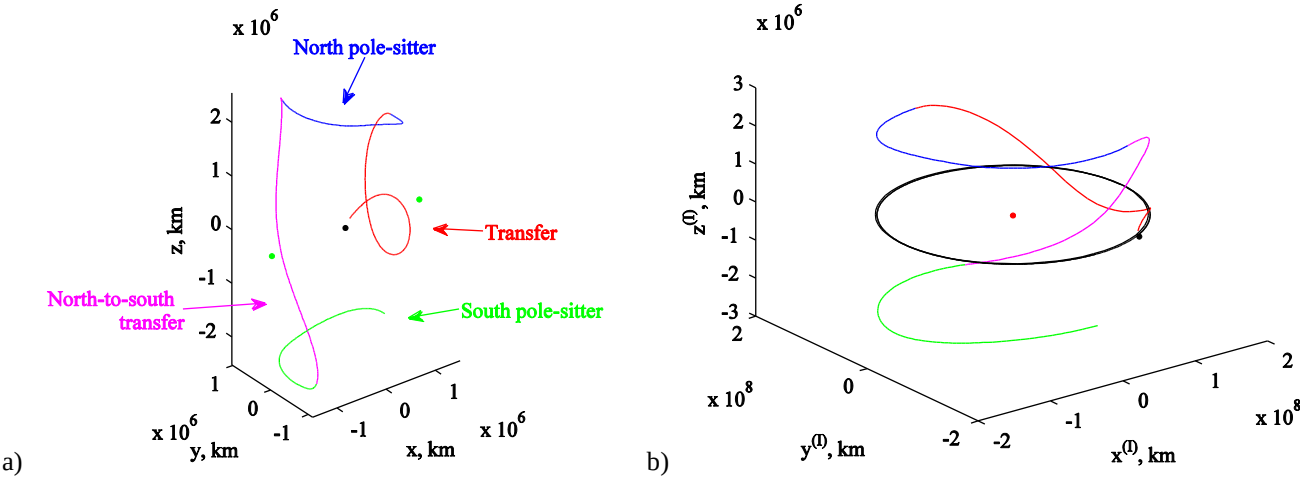

Fig. 12 Hybrid propulsion mission trajectory (Ariane 5 launch) in synodic reference frame (a) and inertial Sun-centered reference frame (b).

IV. Orbit Control

The mission trajectories presented before are unstable, i.e. an arbitrary small perturbation in the state leads to an exponential divergence from the nominal orbit. Therefore, it is particularly important to devise a control strategy to keep the spacecraft on-track, to quantify the control effort (in terms of thrust and additional propellant mass) needed and to determine the stability margin of the controlled system.

Moreover, as a representative of the different perturbations that may act on the real system, here we replace the CR3BP by a model that considers the real ephemerides of the Earth by taking into account the eccentricity of its orbit around the Sun. Hence, an additional control component is also necessary to compensate for such effects.

The control loop used here is based on a linear quadratic regulator (LQR) [37], applied in a similar way as in Ref. [38]. As a result of the trajectory design in the previous sections, we obtained the *reference* state (position, velocity) and control (thrust) histories $\mathbf{x}_r(t), \mathbf{u}_r(t)$ respectively. In an ideal condition, the real state coincides with the reference one. However, due to the instability of the trajectory, the different dynamical model (real ephemerides of the Earth), or other sources of error, the real state may differ from the reference one, and therefore the state error can be defined as: $\delta\mathbf{x} = \mathbf{x} - \mathbf{x}_r$. The objective of the controller is to find the additional component of control, $\delta\mathbf{u}$ (defined as the feedback control) such that the total control $\mathbf{u} = \mathbf{u}_r + \delta\mathbf{u}$ brings the spacecraft states back to the reference states after some time.

As actuator for the control loop, we only use the SEP thruster. This means that the SEP thrust is varied with respect to the reference, while the sail attitude is kept unchanged. Despite that this can result in a higher propellant consumption, because in general the sail is not tilted optimally following a perturbation, we can assume that there is no time delay in the actuator. Tilting a large solar sail can in fact require a relatively long duration, due to the large moments of inertia, while activating the thrusters can be considered instantaneous, compared to the dynamics of the orbit. Also, we assume that the spacecraft has perfect knowledge of its state vector at any time. Note that $\mathbf{u}$ is subject to saturation according to the maximum thrust values presented in Table 2. The resulting thrust is then fed into the integration of the full equations of motion, modified to include the real ephemerides of the Earth and the Sun, computed through an analytic approximation of the JPL/NAIF/SPICE ephemerides de405.bps. Note that the control effort can be reduced by re-optimizing the trajectory using ephemeris data, but the intention is to demonstrate the robustness of the control.

The results presented in the following refer to the launch with Ariane 5. The control performs in a very similar way when the Soyuz reference trajectories are used, after re-scaling the mass and the maximum thrust according to Table 2. These test cases are not meant to be exhaustive, but rather to give an indication of the performance and the fuel requirement of the controller. In all time-history plots in this section, the two shaded areas represent the transfer phases, from Earth to pole-sitter and north to south, respectively.

A. Results: nominal conditions

Firstly, we evaluated the performance of the feedback controller when the spacecraft is injected into the transfer trajectory within nominal conditions. Fig. 13 shows a comparison between the reference solution and the solution with real

ephemerides and feedback control, for the SEP spacecraft. The first plot (a) represents the three components of the error with respect to the reference in position ($\delta\mathbf{x}_{1,2,3}$): it can be seen that the feedback controller maintains the spacecraft within 50,000 km from the reference, along each axis. It resulted that the velocity error is limited to and 15 m/s. These values are relatively small compared to the reference pole-sitter orbit and transfer. Nevertheless, the controller could be designed with tighter requirements, at the cost of additional propellant consumption and actuator effort. Fig. 13 (b) shows the magnitude of the thrust in the reference solution (dashed line) and in the feedback-controlled solution (solid line). The contribution to the thrust added by the feedback controller is evident. Note that the transfer phases, Earth to pole-sitter and north-to-south, contain ballistic arcs in the reference solution, while in the same arcs the feedback controller provides a continuous, albeit small thrust, with a high-frequency component to compensate for instabilities. Moreover, along the thrust arcs, the feedback-controlled trajectory requires either less or more thrust than the reference one, and this is mainly due to the effect of the eccentricity of the Earth. It resulted that 12 kg of additional fuel are required by the feedback controller, over the part of the mission considered.

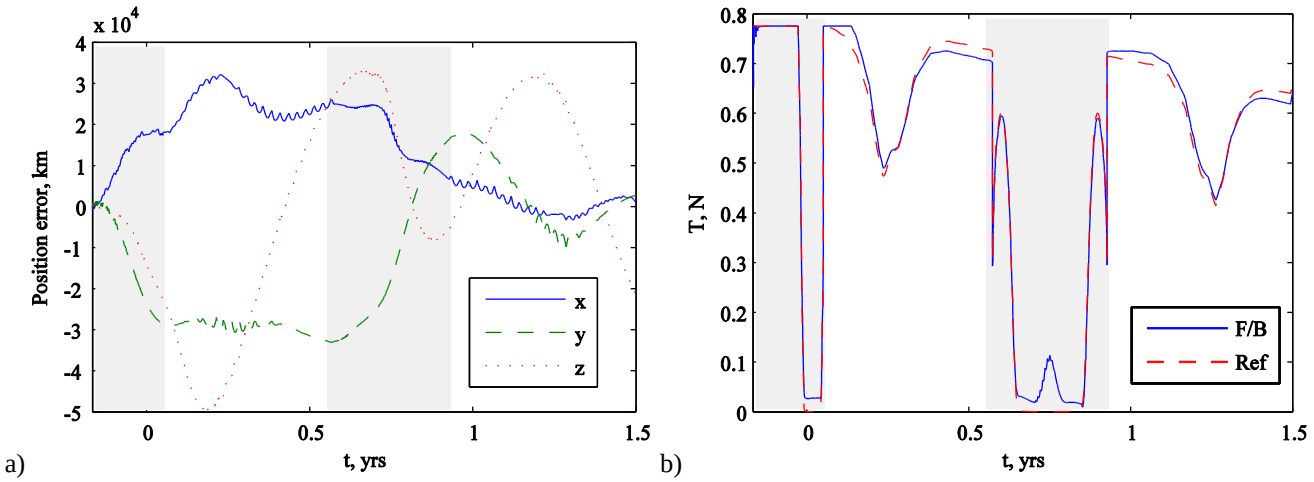

Fig. 13 Comparison between reference solution and feedback-controlled solution. SEP, Ariane 5 case. (a) Position error with respect to the reference; (b) SEP thrust magnitude. Shaded areas are transfer phases.

In the case of the hybrid propulsion spacecraft, similar performances are obtained in terms of displacement from the reference orbit. The propellant consumption is higher than for the SEP spacecraft: 40 kg of additional fuel are required for controlling the trajectory. The higher fuel consumption is due to the fact that the distance from the Sun varies, due to the eccentricity of the Earth's orbit, and this is affecting not only the gravitational acceleration, but also the acceleration produced by the solar sail. Again, we note that ephemeris data is used to demonstrate robustness of the controller. In

addition, the Earth to pole-sitter transfer is considerably longer for the hybrid spacecraft, and despite this phase is nearly ballistic in the reference solution, it requires a non-negligible amount of SEP thrust from the controller.

B. Results: launcher injection error

In this second scenario, we assume the spacecraft is injected into the transfer trajectory (i.e. at the end of the launch phase) with a given error in position and velocity. In this test, we consider again the Ariane 5 launch with an SEP-only spacecraft, however we introduce a change in the initial states (in the synodic reference frame) of $\delta r_x = -100{,}000$ km; $\delta v_z = -100$ m/s .

Fig. 14 (a) shows again the errors with respect to the reference for each position component of the state vector. It can be seen that the correction of the initial position and velocity errors leads to overshooting in other components of the state (including velocity, not shown). The large initial error in position can be appreciated from the plot of the reference and feedback trajectory in the Earth-centered synodic frame in Fig. 14 (b). Fig. 14 (c) show the SEP thrust, and the additional thrust required during the transfer and immediately after, to correct the injection error, is evident; it results that 22 kg of additional propellant mass are required. This is to be compared with the 12 kg needed in the case where no injection error was present. It is worth underlining that without feedback controller, injection errors much smaller than those considered are enough to prevent the spacecraft from reaching the pole-sitter orbit.

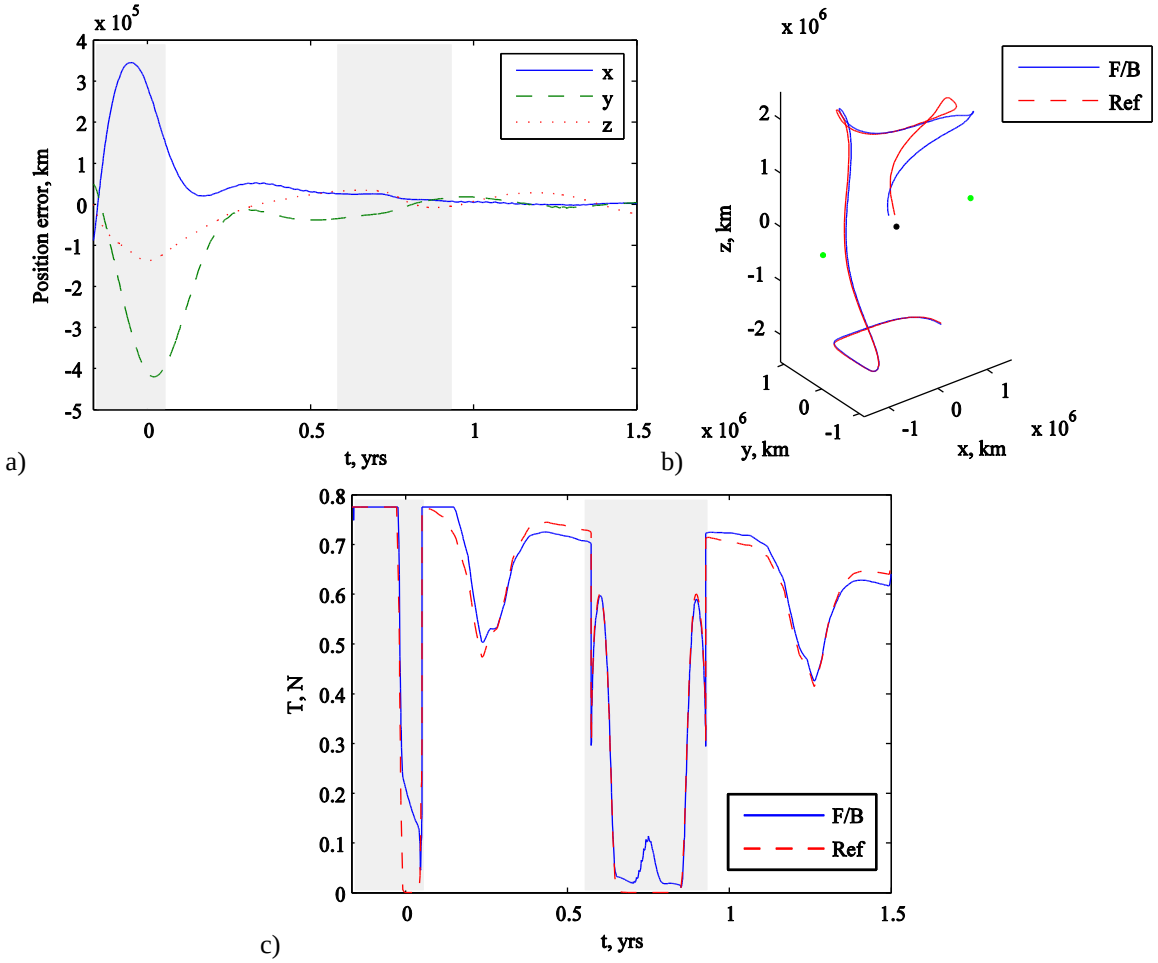

Fig. 14 Comparison between reference solution and feedback-controlled solution. SEP, Ariane 5 case with injection error. (a) Position error with respect to the reference; (b) Trajectory in Earth-centered synodic frame; (c) SEP thrust magnitude. Shaded areas are transfer phases.

The effect of injection errors was tested also on the hybrid propulsion spacecraft injected by the Ariane 5 upper-stage, this time with an error of: $\delta r_z = 10{,}000$ km; $\delta v_y = 100$ m/s. In this case, the control brings back the states to the proximity of the reference states during the transfer itself, thanks also to the longer transfer time, and the total additional mass of the controlled solution with injection error is approximately 60 kg.

As a final remark to conclude this section on feedback control: again, the controlled solution would require less propellant mass if the reference solutions were re-optimized considering the real ephemerides of the Earth, rather than the CR3BP model. In this case, the feedback control would cope only with instabilities and contingencies.

V. Spacecraft Design

A. Spacecraft Subsystems Sizing

Now that the mass that can be injected into the operational orbit of the pole-sitter is known, a systems design provides the mission lifetime that can be achieved into this orbit, or alternatively the payload mass that can be carried for a given lifetime of the spacecraft. This estimation is the subject of this section.

The total mass of the pure SEP spacecraft (carrying a payload mass m_{pl}, to be determined) can be defined as:

$$m_0 = \left[m_{prop} + m_{tank} + n_{thrusters} m_{thruster} + m_{SA} + m_{other} \right] \left(1 + \varepsilon_{old}\right) + m_{pl} \tag{3}$$

and for the hybrid propulsion spacecraft:

$$\begin{aligned} m_0 = &\left[m_{prop} + m_{tank} + n_{thrusters} \left(m_{thruster} + m_{gimbal} \right) + m_{rad} + m_{other} \right] \left(1 + \varepsilon_{old}\right) + \\ &+ \left[m_s + m_{TF} \right] \left(1 + \varepsilon_{new}\right) + m_{pl} \end{aligned} \tag{4}$$

Formulas defining all the terms in these equations are grouped in Table 3 for convenience. Here we provide only a description of each term in Eqs. (3) and (4).

m_{prop} is the propellant mass required for a certain mission lifetime. The mass of the propellant tanks m_{tank} is computed as a fraction of this mass.

The mass of each SEP thruster, $m_{thruster}$, is proportional to its power, and takes into account the control units and cabling related to the SEP subsystem. The sizing is done based on the maximum power $P_{SEP,max}$ required by the SEP subsystem, which is in turn a function of the maximum thrust T_{max} required during the mission.

In the hybrid spacecraft, the sail, fixed to the spacecraft bus, determines the attitude of the bus itself. Therefore, a gimbal system is required to point the thrust vector independently from the attitude of the spacecraft (within limits due to the system configuration). m_{gimbal} is the SEP thruster gimbal mass, and it is assumed to be proportional to the thruster mass. Instead, for the pure SEP spacecraft, no gimbal is used, as the attitude of the three-axis stabilized spacecraft can be changed to orientate the thrust vector in the required direction. Note that the mass of the SEP subsystem does not depend on the number of thrusters, provided that all of them contribute equally to the thrust.

For the pure SEP spacecraft, the mass of the solar array m_{SA} is proportional to its area A_{SA}. The area of the solar array can be estimated as a function of the maximum power, considering that the solar panels are usually kept perpendicular to the Sun vector, and their efficiency η_{SA}. The energy flux density of the Sun $W = 1367\ \mathrm{W/m^2}$ is considered constant at 1 AU.

As noted, for the hybrid spacecraft we foresee the use of TFSC covering part of the sail assembly to generate power for the SEP thruster. Analogously to the solar array, the mass is proportional to the area. In addition, they have a pitch angle with respect to the Sun vector equivalent to that of the sail, and this is taken into account when computing the effective area. The efficiency of the solar array is higher than that of the TFSC, but their mass per unit area is also higher.

The solar arrays and TFSC are sized on the maximum power needed, assuming that they can be maintained perpendicular to the Sun in the pure SEP spacecraft, and at the sail attitude for the hybrid spacecraft. However, the thrust, and hence the power required during the whole mission is variable. It was found that for some configurations, the full SEP thrust is not needed for long durations during the orbit (around summer). In these cases, while the solar panels of the SEP spacecraft can be tilted, such that they generate only the power needed at each instant in time, this is not possible for the hybrid spacecraft. The attitude of the TFSC is once again constrained to that of the sail, and therefore they will produce power. Radiators can be employed to dissipate the excess power. Such radiator mass m_{rad} is sized considering the minimum SEP thrust throughout the mission, and calculating the excess of power $P_{d,max}$ generated by the panels at that instant of time, and so the power that is to be dissipated. Radiators are assumed to have a specific power of 350 W/m^2 (value achievable in deep space [1] (p. 440)), and a specific mass of 3 kg/m^2, considering that they can be mounted on the back side of the TFSC, sharing the structure; from these values, the coefficient in Table 3 can be found. The pure SEP spacecraft does not need radiators for the reasons stated above.

The total sail area (highly reflective surface plus TFSC), A, can be computed starting from the assumed value of β_0 and the optimized value for m_0. The area of the reflective part of the solar sail is simply $A_s = A - A_{TF}$, and its mass is proportional to the mass per unit area of the sail σ_s, as discussed in Section II.B.

The mass of all the other subsystems m_{other} (ADCS, thermal, structure, OBDH, TT&C) is estimated as a fraction of the spacecraft dry mass m_{dry}.

Margins are taken into account for each subsystem [1]. In particular, the sail and the thin film solar cells are considered new technologies, and therefore a margin of $\varepsilon_{new} = 0.20$ is used. Conversely, the other subsystems are considered to be well-proven technologies, and its margin is set to $\varepsilon_{old} = 0.05$. Note that the same margin is added to the propellant mass for contingency maneuvers. Table 3 and Fig. 15 summarize the formulas and subsystems used for each configuration, highlighting the differences between the pure SEP and the hybrid spacecraft.

Note that the systems mass budget proposed here differs to the one in Ref. [20] in several ways: it considers multiple SEP thrusters, but working in parallel to achieve the necessary thrust, rather than being redundant; the mass of the other

subsystems is now taken into account, and not considered as "payload" mass; the pure SEP spacecraft does not employ thin film solar cells, but solar arrays mounted on panels (higher efficiency and areal mass); the pure SEP spacecraft does not employ a gimbal system, as it is assumed that attitude maneuvers can be used to steer the thrust vector; lastly, margins are taken into account.

Table 3 Formulas for the subsystem mass budget in Eqs. (3) and (4) for the pure SEP and the hybrid spacecraft.

	Pure SEP	Hybrid
Tank mass	$m_{tank} = 0.1 m_{prop}$	
Maximum SEP power	$P_{SEP,max} = T_{max} I_{sp} g_0 / 2\eta_{SEP}$ $\eta_{SEP} = 0.7$ [35]	
SEP thruster (each)	$m_{thruster} = k_{SEP} P_{SEP,max} / n_{thrusters}$ $k_{SEP} = 20\,\mathrm{kg/kW}$ [25]	
SEP thruster gimbal	N/A	$m_{gimbal} = \rho_{gimbal} m_{thruster}$ $\rho_{gimbal} = 0.3$ [36]
Solar arrays (thin film solar cells or solar panels)	$A_{SA} = P_{SEP,max} / W\eta_{SA}$ $\eta_{SA} = 0.10$	$A_{TF} = P_{SEP,max} / W\eta_{TF} \cos\alpha_{T_{max}}$ $\eta_{TF} = 0.05$
	$m_{SA} = \sigma_{SA} A_{SA}$ $\sigma_{SA} = 5.468\ \mathrm{kg/m^2}$ [1]	$m_{TF} = \sigma_{TF} A_{TF}$ $\sigma_{TF} = 100\ \mathrm{g/m^2}$ [11]
Solar sail	N/A	$A_s = A - A_{TF}$ $m_s = \sigma_s A_s$
Radiators	N/A	$m_{rad} = 0.0086\,\mathrm{kg/W} \cdot P_{d,max}$ [1]
Dry mass	$m_{dry} = m_0 - m_{prop}$	
Other subsystems	$m_{other} = 0.3 m_{dry}$ [1]	

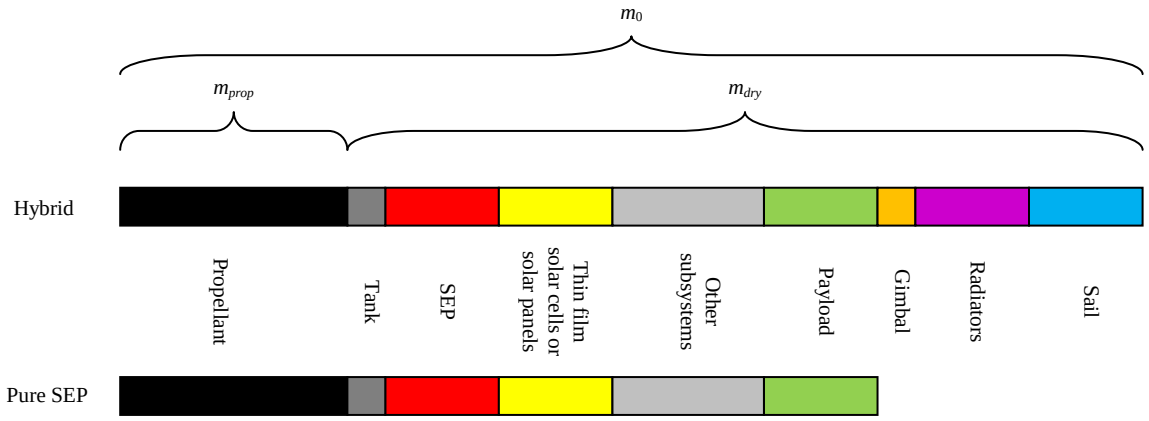

Fig. 15 Mass break-up model for the pure SEP spacecraft and the hybrid spacecraft.

Given the initial mass of the spacecraft in the pole-sitter orbit (as found in Table 2 for a given mission scenario), the optimal 1-year trajectory is used to compute the propellant mass m_{prop} needed for a given lifetime $t_{mission}$. Despite that the same trajectory is flown year after year, the controls are re-optimized locally, step by step, such that the SEP thrust is

minimized point-wise, and hence the propellant consumption is minimum, on that trajectory. Once the propellant mass is found, Equations in Table 2 followed by Eq. (3) or (4) can be used to compute the payload mass m_{pl}. This is plotted, as a function of the lifetime, in Fig. 16. Each plot refers to one spacecraft architecture (pure SEP, hybrid).

It can be noted that the maximum mission lifetime (i.e. no payload carried on-board) does not depend on the injection total mass m_0, but only on the technology that is used to build the spacecraft. The lifetime for the pure SEP system is limited to approximately 4.5 years, while this value extends to about 7 years for the hybrid architecture. This result itself should be sufficient to justify the interest in the hybrid propulsion technology for this type of mission, and in general for all those missions which require a continuous acceleration [20]. Furthermore, for nearly equal injected masses, the hybrid spacecraft can carry the same payload mass for a longer mission lifetime. Finally, for a particular spacecraft architecture and a given lifetime, the payload mass scales with the injected mass m_0.

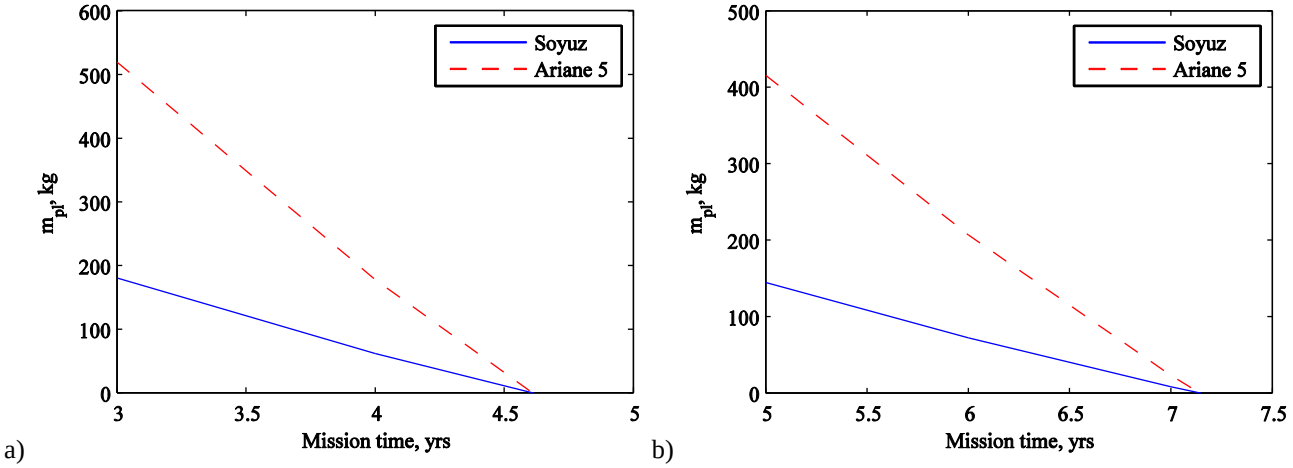

Fig. 16 Payload mass (m_{pl}) as a function of the mission lifetime, for the pure SEP spacecraft (a) and the hybrid spacecraft (b).

By fixing a payload mass, e.g. 100 kg, the design points for the four scenarios can be computed, and they are described in Table 4. The value of 100 kg will be justified in the following Section B. The design points are computed assuming that the entire capacity of the launcher is used for the pole-sitter spacecraft; however, it is possible to scale down any of the four scenarios (at the cost of a reduction in mission lifetime).

Launching with Soyuz, the lifetime is 3.6 years if the spacecraft is using pure SEP technology, or 5.6 years if using hybrid propulsion. These lifetimes extend to 4.2 and 6.6 years when launching with Ariane 5 for the two architectures respectively.

The subsystem design also allows the computation of the mass of the other subsystems, some of which are reported in Table 4. The size of the total sail assembly (reflective surface and thin film solar cells) of the hybrid spacecraft, assuming a square assembly, is 191 × 191 m^2 for the Soyuz launch, and 324 × 324 m^2 for the Ariane launch.

The hybrid configuration furthermore allows a lower power budget, by reducing the thrust needed per unit mass of the spacecraft from the SEP thruster. For the pure SEP spacecraft, the maximum power required by the SEP thruster is 6 kW (Soyuz) and 17.4 kW (Ariane 5). For the hybrid, instead, the power is 5.2 kW (Soyuz) and 15 kW (Ariane 5), despite the fact that the total injected mass of the spacecraft, m_0, is slightly larger than in the SEP case.

Table 4 Design points for 100 kg payload mass. Masses are without margins.

Architecture	Pure SEP		Hybrid	
Launcher	Soyuz	Ariane 5	Soyuz	Ariane 5
Lifetime, $t_{mission}$, yrs	3.6	4.2	5.6	6.6
Payload mass, m_{pl}, kg	100	100	100	100
Pole-sitter injected mass, m_0, kg	1537	4439	1595	4599
SEP mass, $n_{thrusters} m_{thruster}$, kg	121	348	104	299
Propellant mass, m_{prop}, kg	675	2192	698	2242
Other subsystems mass, m_{other}, kg	259	674	269	707
Solar array or TFSC area, A_{SA} or A_{TF}, m^2	44	127	121	349
Solar sail mass (reflective), m_s, kg	-	-	182	524
Total sail area (reflective + TFSC), A, m^2	-	-	191 × 191	324 × 324
Maximum SEP thrust, T_{max}, mN	269	776	231	667
Maximum SEP power, $P_{SEP,max}$, kW	6	17.4	5.2	15.0

B. Payload Selection and Sizing

We now wish to investigate possible payloads that could be used on the pole-sitter spacecraft. The pole-sitter spacecraft could serve as a platform for Earth observation and science, and a data relay for telecommunications. Concerning the former, taking into account the considerable distance of the spacecraft from the Earth, high-resolution imaging is limited to the near-visible part of the spectrum (from infrared to ultra-violet). Spatial resolution in the visible wavelength in the range 10-40 km should be available, which enables real-time, continuous views of dynamic phenomena and large-scale polar weather systems [19]. The creation of atmospheric motion vectors (AMV) would also make use of the stationary location of the platform, avoiding gap problems related to geolocation and intercalibration that composite images introduce [5]. Glaciology and ice-pack monitoring would also benefit from continuous, but low resolution polar observation [5]. Ultraviolet imagery of the polar night regions at 100 km resolution or better would enable real-time monitoring of rapidly-

changing hot spots in the aurora that can affect high frequency communications and radar [19]. As the resolution degrades with increasing wavelength, it is unlikely that sensing in the microwave band could provide some useful information. However, radio science can detect the total flux of radiation reflected and emitted by the Earth at the poles.

Candidate instruments for continuous polar observations are found in the literature for deep space missions. In fact, optics for deep space mission typically have long focal lengths and narrow field of views (FOVs), and they are therefore ideal for the pole-sitter. Table 5 collects a number of instruments that were designed for three past missions. In particular, the NASA mission Galileo, launched in 1989 towards Jupiter and its satellites, was designed to perform observations of Jupiter's atmospheric composition, weather phenomena and auroras. Despite that the instruments used on this spacecraft are now outdated, they provide an indication of the data, mass and resolution of the instruments suitable for pole-sitter distances (Fig. 17). The NASA Deep Space Climate Observatory (DSCOVR) mission was designed for Earth observation and science from the L_1 Lagrange point, which is located approximately 1.5 million km from the Earth, of the same order as the distance of the pole-sitter mission (where angular size of the Earth disc is approximately 0.5 deg). Unfortunately, this mission was canceled before launch; nevertheless, its payload would be similar to what could be used on a pole-sitter spacecraft. Finally, a compact, modern instrument for imaging in the visible and infrared range was successfully flown on the Deep Impact mission. A complete discussion on potential applications enabled by such instrumentation is found in Ref. [2].

Table 5 shows the resolution, wavelength, aperture (to provide an estimate of the size of the instrument), mass and power of each instrument, as well as the main objectives of the instrument within their original mission. The table is interesting as it shows that for all the instruments, the total mass is of the order 50 kg. Therefore, based on Fig. 16, they are all suitable for both hybrid and SEP configurations missions, for lifetimes of about 4 years or more.

From the same table it can be noted that the power needed by any of these instruments is two orders of magnitude lower than the power required by the SEP thruster, and therefore should not constitute a strong constraint in the power budget.

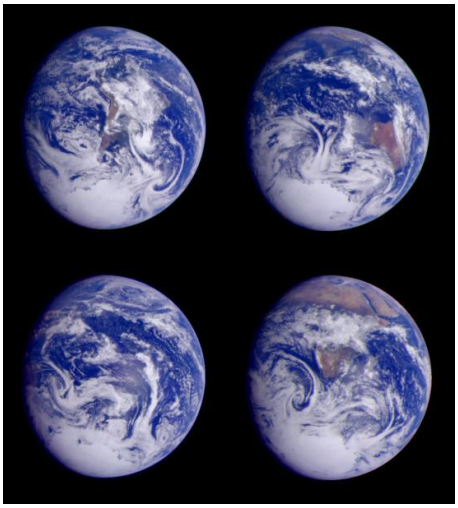

Fig. 17. Four views of the Earth as taken by Solid-State Imaging instrument on Galileo spacecraft during its first Earth fly-by, at six-hour intervals on December 11, 1990, at a range of between 2 and 2.7 million kilometers. Each disc is about 500×500 pixels. (Credit: NASA, Johns Hopkins University, http://photojournal.jpl.nasa.gov/catalog/PIA00728)

Table 5 Potential Earth observation instruments that could be used for polar observation. Mass and power are also listed, when data are available. Data extracted from the official websites of the programs managing agencies. Notes: * Spatial resolution at Nadir from 2.74 million km; † Spacecraft mass: 650 kg; ‡ Total payload power: 92 W

Instrument	Primary objectives	Pixel matrix size/ Field of View/Resolution*	Wavelength	Aperture/ Diameter	Mass, kg	Power
NASA Galileo Primary objective: Study Jupiter and its Moons (1989)						
Solid State Imaging (SSI)	• Cloud structure • Auroral phenomena	800x800 FOV = 0.46 deg (10.16 μrad/pixel) 27 km	Near visible 404-986 nm	30 cm (f/8.5)	29.7 kg	23 W
Near-Infrared Mapping Spectrometer (NIMS)	• Measure reflected sunlight and emitted thermal radiation • Cloud structure	1x20 0.5x10 mrad (0.5 mrad/pixel) 137 km	Infrared 0.7-5.2 μm	22.9 cm (f/3.5)	18 kg	12 W
Ultraviolet Spectrometer (UVS)	• Composition and structure of upper atmosphere	FOV = 0.17 deg	113-432 nm	25 cm	9.7 kg	5.9 W
Photopolarimeter radiometer (PPR)	• Temperature of atmosphere • Distribution of clouds • Distribution of reflected and emitted thermal radiation	FOV = 2.5 mrad	410-892 nm	10 cm	5 kg	11 W
NASA Deep Impact Study the composition of the comet interior of 9P/Tempel (2005)						
High Resolution Instrument (HRI) CCD	• Observe comet nucleus and impact	1008x1008 FOV = 0.118 deg (2 μrad/pixel) 5.4 km	Visible	30 cm (f/35)	N/F†	N/F‡
High Resolution Instrument (HRI) IR spectrometer	• Spectral reflectivity and thermal emission of the nucleus and dust	2.53 mrad x 10 μrad	Infrared 1.05-4.8 μm	f/12	N/F†	N/F‡
NASA Deep Space Climate Observatory (DSCOVR) (formerly Triana) Observation of Sun-lit side of the Earth's disc from L_1 (proposed in 1998)						
Earth Polychromatic Imaging Spectrometer (EPIC)	• Ozone • Aerosols • Cloud fraction, thickness, optical depth, and height • Sulfur dioxide • Precipitable water vapor • Volcanic ash • UV irradiance	2048x2048 FOV = 0.62 deg (5.3 μrad/pixel) 14.5 km	Near visible	30.5 cm aperture	39 kg (65 kg with computer)	62 W with computer
Active cavity radiometer (NISTAR)	• Emitted and reflected Earth radiation	FOV = 1 deg	0.2-200 μm	N/A	23.5 kg	N/F

Concerning the use of the pole-sitter for telecommunications, the main application would be its use as a low-bandwidth data relay with polar regions, and may be particularly useful in the southern hemisphere, where there are key Antarctic research activities ongoing and communication capabilities are limited. McInnes and Mulligan [5] envisaged possible applications including data links for scientific experiments, links to automated weather stations, emergency airfields and telemedicine. In the same work, the authors proposed the use of polar stationary spacecraft as data relay for future NOAA polar orbiting satellites, such as the NPOESS system. Lastly, a polar-sitter type platform could also be used for high latitude ship tracking and telecommunications, and to support future high-latitude oil and gas exploration, especially if northern sea routes open due to climate change.[*] Again, a complete discussion of possible applications is presented in Ref. [2].

In these cases, the telecommunication subsystem would be the main payload of the spacecraft. However, even for Earth science, there will be a need to download a relatively large volume of data from the spacecraft to the Earth real-time (high resolution imaging, for example). Considering the distance of the pole-sitter from the Earth, a high-gain steerable antenna will be required for either or both of these tasks. Table 6, taken from Ref. [1], shows the mass of some parabolic dishes which were used on telecommunication satellites, together with their mass.

Table 6 Examples of high-gain antennas of telecommunication spacecraft.

Satellite	Type	Band, Frequency	Gain, dBi	Mass, kg	Diameter, m
Intelsat-V	Parabola with Feed Array	C, 4 GHz	21-25	29.4	2.44
Intelsat-V	Parabola with Feed Array	C, 6 GHz	21-25	15.2	1.56
Intelsat-V	Parabola-Steerable	Ku, 11 GHz	36	5.8	1.1
SUPERBIRD	Parabola with Feed Array	Ka, 20/30 GHz	45-52	47.1	1.7

An accurate determination of the mass of the telecommunication subsystem and the observation payload would require the definition of precise mission objectives, temporal and spatial resolution of the images, and an estimation of the required data-rate. However, according to what is shown in this section, we can conclude that the value (previously estimated) of 100 kg for both observation and telecommunication payloads is reasonable.

VI. Conclusions

In this paper a full, preliminary mission analysis and systems design of a near-term and far-term pole-sitter mission is provided, where the distinction comes from the use of either existing, solar electric propulsion or more far-term hybrid solar-electric and solar sail propulsion. The platform would provide a vantage view point on either pole of the Earth, with essentially unlimited temporal resolution (real-time observations) by means of one spacecraft only. Optimal transfers from

[*] http://www.esa.int/esaEO/SEMT7TRTJRG_index_0.html [cited 12/09/2011].

north to south and vice-versa have been shown to be feasible and allow observation of the pole that is lit, at no extra cost in terms of propellant consumption. Moreover, in some particular cases propellant savings were achieved through the use of these transfers, allowing for an extension of the mission lifetime or alternatively an increase in the payload mass.

Despite the considerable distance of the spacecraft from Earth, a set of instruments used on the Galileo mission and others designed for the Deep Space Climate Observatory Earth observation mission from Lagrange point L_1 were shown to enable the observation of large-scale, rapidly-changing weather phenomena, aurorae, ice-pack dynamics, and other phenomena that require only modest spatial resolution. It was also shown to be feasible to employ a high-gain antenna to use the spacecraft as a continuous data-relay with scientific stations in the Antarctic and other high-latitude users. Using the full potential of either a Soyuz or Ariane 5 launch vehicle, a systems mass budget demonstrated that it is potentially possible to deliver these payloads with a mass of 100 kg for at least 4 years for the short-term solar-electric mission, and 6 years or more for the far-term hybrid mission. Any influences of the real ephemeris of the Earth during the mission or errors such as launcher injection errors have been shown to be controllable with a linear feedback controller.

Acknowledgements

This work was funded by the European Research Council, as part of project 227571 VISIONSPACE. The authors thank Dr. Victor M. Becerra, of the School of Systems Engineering, University of Reading, Reading, UK for providing the software PSOPT freely, as well as advices on its use. Many thanks also to Alex Coletti, of SMRC, for valuable discussions on instruments for polar observation and for providing some of the data presented in this paper.

References

[1] Wertz, J. R. and Larson, W. J. (eds.), *Space Mission Analysis and Design, Third Edition*, Space Technology Library, Microcosm press/Kluwer Academic Publishers, El Segundo, California, USA, 1999.

[2] Ceriotti, M., Diedrich, B. L. and McInnes, C. R., "Novel Mission Concepts for Polar Coverage: An Overview of Recent Developments and Possible Future Applications," *Acta Astronautica*, Vol. 80, 2012, pp. 89-104.
doi: 10.1016/j.actaastro.2012.04.043

[3] Anderson, P. C. and Macdonald, M., "Extension of the Molniya Orbit Using Low-Thrust Propulsion," *21st AAS/AIAA Space Flight Mechanics Meeting*, AAS 11-236, AIAA, New Orleans, USA, 2011.

[4] Anderson, P. C. and Macdonald, M., "Extension of Earth Orbits Using Low-Thrust Propulsion," *61st International Astronautical Congress (IAC 2010)*, Prague, Czech Republic, 2010.

[5] McInnes, C. R. and Mulligan, P., "Final Report: Telecommunications and Earth Observations Applications for Polar Stationary Solar Sails," National Oceanographic and Atmospheric Administration (NOAA)/University of Glasgow, Department of Aerospace Engineering, 2003, www.osd.noaa.gov/rpsi/polesitter.telecommunications.pdf [retrieved 16 November 2010].

[6] Driver, J. M., "Analysis of an Arctic Polesitter," *Journal of Spacecraft and Rockets*, Vol. 17, No. 3, 1980, pp. 263-269.
doi: 10.2514/3.57736

[7] McInnes, C. R., *Solar Sailing: Technology, Dynamics and Mission Applications*, Springer-Praxis Books in Astronautical Engineering, Springer-Verlag, Berlin, 1999.

[8] Waters, T. J. and McInnes, C. R., "Periodic Orbits above the Ecliptic in the Solar-Sail Restricted Three-Body Problem," *Journal of Guidance, Control, and Dynamics*, Vol. 30, No. 3, 2007, pp. 687-693.
doi: 10.2514/1.26232

[9] Forward, R. L., "Statite: A Spacecraft That Does Not Orbit," *Journal of Spacecraft and Rockets*, Vol. 28, No. 5, 1991, pp. 606-611.
doi: 10.2514/3.26287
[10] McInnes, C. R., McDonald, A. J., Simmons, J. F. L. and MacDonald, E. W., "Solar Sail Parking in Restricted Three-Body Systems," *Journal of Guidance, Control, and Dynamics*, Vol. 17, No. 2, 1994, pp. 399-406.

[11] Leipold, M. and Götz, M., "Hybrid Photonic/Electric Propulsion," Kayser-Threde GmbH, Technical Report SOL4-TR-KTH-0001, ESA contract No. 15334/01/NL/PA, Munich, Germany, 2002, January 2002.
[12] Baig, S. and McInnes, C. R., "Artificial Three-Body Equilibria for Hybrid Low-Thrust Propulsion," *Journal of Guidance, Control, and Dynamics*, Vol. 31, No. 6, 2008, pp. 1644-1655.
doi: 10.2514/1.36125
[13] Mengali, G. and Quarta, A. A., "Trajectory Design with Hybrid Low-Thrust Propulsion System," *Journal of Guidance, Control, and Dynamics*, Vol. 30, No. 2, 2007, pp. 419-426.
doi: 10.2514/1.22433
[14] Mengali, G. and Quarta, A. A., "Tradeoff Performance of Hybrid Low-Thrust Propulsion System," *Journal of Spacecraft and Rockets*, Vol. 44, No. 6, 2007, pp. 1263-1270.
doi: 10.2514/1.30298
[15] Simo, J. and McInnes, C. R., "Displaced Periodic Orbits with Low-Thrust Propulsion," *19th AAS/AIAA Space Flight Mechanics Meeting*, AAS 09-153, American Astronautical Society, Savannah, Georgia, USA, 2009.

[16] Heiligers, J., Ceriotti, M., McInnes, C. R. and Biggs, J. D., "Displaced Geostationary Orbit Design Using Hybrid Sail Propulsion," *Journal of Guidance, Control, and Dynamics*, Vol. 34, No. 6, 2011, pp. 1852-1866.
doi: 10.2514/1.53807
[17] Macdonald, M. and McInnes, C. R., "Solar Sail Mission Applications and Future Advancement," *2nd International Symposium on Solar Sailing (ISSS 2010)*, edited by R.Y. Kezerashvili, New York, NY, USA, 2010, pp. 7-26.

[18] Ceriotti, M. and McInnes, C. R., "Generation of Optimal Trajectories for Earth Hybrid Pole-Sitters," *Journal of Guidance, Control, and Dynamics*, Vol. 34, No. 3, 2011, pp. 847-859.
doi: 10.2514/1.50935
[19] Lazzara, M. A., Coletti, A. and Diedrich, B. L., "The Possibilities of Polar Meteorology, Environmental Remote Sensing, Communications and Space Weather Applications from Artificial Lagrange Orbit," *Advances in Space Research*, Vol. 48, No. 11, 2011, pp. 1880-1889.
doi: 10.1016/j.asr.2011.04.026
[20] Ceriotti, M. and McInnes, C. R., "Systems Design of a Hybrid Sail Pole-Sitter," *Advances in Space Research*, Vol. 48, No. 11, 2011, pp. 1754–1762.
doi: 10.1016/j.asr.2011.02.010
[21] Heiligers, J., Ceriotti, M., McInnes, C. R. and Biggs, J. D., "Design of Optimal Earth Pole-Sitter Transfers Using Low-Thrust Propulsion," *Acta Astronautica*, Vol. 79, 2012, pp. 253–268.
doi: 10.1016/j.actaastro.2012.04.025
[22] Heiligers, J., Ceriotti, M., McInnes, C. R. and Biggs, J. D., "Design of Optimal Transfers between North and South Pole-Sitter Orbits," *22nd AAS/AIAA Space Flight Mechanics Meeting*, AIAA, Charleston, South Carolina, USA, 2012.

[23] Becerra, V. M., "Solving Complex Optimal Control Problems at No Cost with Psopt," *IEEE Multi-conference on Systems and Control*, IEEE, Yokohama, Japan, 2010, pp. 1391-1396.

[24] Wächter, A. and Biegler, L. T., "On the Implementation of a Primal-Dual Interior Point Filter Line Search Algorithm for Large-Scale Nonlinear Programming," *Mathematical Programming*, Vol. 106, No. 1, 2006, pp. 25-57.

[25] Brophy, J., "Advanced Ion Propulsion Systems for Affordable Deep-Space Missions," *Acta Astronautica*, Vol. 52, No. 2-6, 2003, pp. 309-316.
doi: 10.1016/S0094-5765(02)00170-4
[26] Leiter, H. J., Killinger, R., Bassner, H., Müller, J., Kukies, R. and Fröhlich, T., "Development and Performance of the Advanced Radio Frequency Ion Thruster Rit-Xt," *28th International Electric Propulsion Conference (IEPC 2003)*, Toulouse, France, 2003.

[27] Funase, R., Mori, O., Tsuda, Y., Shirasawa, Y., Saiki, T., Mimasu, Y. and Kawaguchi, J., "Attitude Control of Ikaros Solar Sail Spacecraft and Its Flight Results," *61st International Astronautical Congress (IAC 2010)*, IAF, Prague, Czech Republic, 2010.

[28] Dachwald, B., Mengali, G., Quarta, A. A. and Macdonald, M., "Parametric Model and Optimal Control of Solar Sails with Optical Degradation," *Journal of Guidance, Control, and Dynamics*, Vol. 29, No. 5, 2006, pp. 1170-1178.
doi: 10.2514/1.20313
[29] Kawaguchi, J. i., Mimasu, Y., Mori, O., Funase, R., Yamamoto, T. and Tsuda, Y., "Ikaros - Ready for Lift-Off as the World's First Solar Sail Demonstration in Interplanetary Space," *60th International Astronautical Congress (IAC 2009)*, IAC-09-D1.1.3, International Astronautical Federation, Daejeon, Korea, 2009.

[30] Johnson, L., Whorton, M., Heaton, A., Pinson, R., Laue, G. and Adams, C., "Nanosail-D: A Solar Sail Demonstration Mission," *Acta Astronautica*, Vol. 68, No. 5-6, 2011, pp. 571–575.
doi: 10.1016/j.actaastro.2010.02.008
[31] Murphy, D. M., Murphey, T. W. and Gierow, P. A., "Scalable Solar-Sail Subsystem Design Concept," *Journal of Spacecraft and Rockets*, Vol. 40, No. 4, 2003, pp. 539-547.
doi: 10.2514/2.3975
[32] Starsem, T. S. C., "Soyuz User's Manual (St-Gtd-Sum-01 - Issue 3 - Revision 0)," 2001, http://www.scribd.com/doc/50249992/Soyuz-Users-Manual.
[33] Vallado, D. A., *Fundamentals of Astrodynamics and Applications*, 3rd Edition, Space Technology Library, New York, USA, 2007.
[34] Arianespace, "Ariane 5 User's Manual - Issue 5 Revision 1," Arianespace, 2011, July 2011, http://www.arianespace.com/launch-services-ariane5/Ariane-5-User's-Manual.asp.
[35] Kitamura, S., Ohkawa, Y., Hayakawa, Y., Yoshida, H. and Miyazaki, K., "Overview and Research Status of the Jaxa 150-Mn Ion Engine," *Acta Astronautica*, Vol. 61, No. 1-6, 2007, pp. 360-366.
doi: 10.1016/j.actaastro.2007.01.010
[36] Gershman, R. and Seybold, C., "Propulsion Trades for Space Science Missions," *Acta Astronautica*, Vol. 45, No. 4-9, 1999, pp. 541-548.
doi: 10.1016/S0094-5765(99)00174-5
[37] Bryson, A. E. and Ho, Y.-C., *Applied Optimal Control: Optimization, Estimation, and Control (Revised Printing)*, Taylor & Francis Group, New York, 1975.
[38] Ceriotti, M. and McInnes, C. R., "Hybrid Solar Sail and Solar Electric Propulsion for Novel Earth Observation Missions," *Acta Astronautica*, Vol. 69, No. 9-10, 2011, pp. 809–821.
doi: 10.1016/j.actaastro.2011.06.007